Final Report

for

READ-ONLY MEMORIES

July, 1969

Contract No: NAS5-10610

Prepared by

WESTINGHOUSE DEFENSE AND SPACE CENTER
Aerospace Division
Baltimore, Maryland 21203

for

GODDARD SPACE FLIGHT CENTER
National Aeronautics and Space Administration
Greenbelt, Maryland 20771

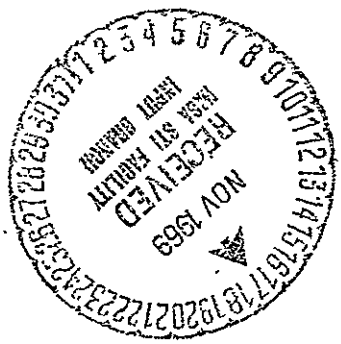

Final Report

for

READ-ONLY MEMORIES

July, 1969

Contract No: NAS5-10610

Goddard Space Flight Center

Technical Monitor: David H. Schaefer

Prepared by

J.R. Cricchi, W. S. Lytle, D.D. O'Sullivan
WESTINGHOUSE DEFENSE AND SPACE CENTER
Aerospace Division
Baltimore, Maryland 21203

for

GODDARD SPACE FLIGHT CENTER
National Aeronautics and Space Administration
Greenbelt, Maryland 20771

ABSTRACT

The objective of the Read-Only Memories Program was to develop integrated low-power MOS memories having nonvolatile and electrically programmable characteristics. Four-bit CMOS memory cells, using fusible link memory elements in one case and oxide breakthrough memory elements in another, were developed. Low-current threshold fusible link elements, having pulse currents of less than 10 mA and current interrupt times of less than 100 microseconds, were achieved. A heat-flow analysis and repeated evidence of metal migration from the cathode support the theory of thermally accelerated electromigration as a dominant fusing mechanism. Also, oxide breakthrough memory elements, having reproducible breakdown voltages of 20 volts and linear contact resistance of less than 200 ohms after breakdown, were achieved. Thermal instability is also a factor in the oxide breakthrough elements. The conclusion is that electrically programmable MOS memory cells with either or both of these elements may be intergrated as large scale arrays.

TABLE OF CONTENTS

LIST OF ILLUSTRATIONS

LIST OF TABLES

1. INTRODUCTION AND SUMMARY

The objective of the Read-Only Memories Program (NAS 5-10610) was to develop integrated complementary MOS read-only memories compatible with the low-power read/write volatile memories developed under the Integrated Circuit Memory Program (NAS 5-10243). The read-only memorie differ in that they are nonvolatile, and they are electrically programmable.

The approach in the first phase of the program, covered by this report, emphasized investigations to determine the effect of processing techniques and parameters on the characteristics of fusible link and oxide breakthrough memory elements. All of the techniques and processes used are compatible with the fabrication of MOS arrays. Low-current threshold fusible link elements, having pulse current thresholds of less than 10 mA and current interruption times of less than 100 microseconds, were achieved, even though the physical configuration was not optimized. The most reproducible low-current threshold was obtained using the constricted chromimum - chrominum oxide film on aluminum contacts. The conclusion is the low-current threshold is principally the result of thermally accelerated electro-migration at the constriction. The heat transfer analysis, the tendency towards localized thermal runaway, and the repeated evidence of migration from the cathode support this conclusion. Oxide breakthrough memory elements having reproducible breakdown voltages of 20 volts and linear and reliable contact resistance of less than 200 ohms, after programming, were also achieved. Single-point oxide breakthrough with typically 0.5-micrometer diameter was obtained by controlling the energy of the break-down pulse.

Four-bit CMOS memory cells, using the oxide breakthrough element in one case and fusible link elements in another, were built, in breadboard form, and delivered. The conclusion is that electrically programmable MOS memory cells, using either or both of these two elements, may be integrated as large scale arrays.

2. TECHNICAL DISCUSSION

2.1 PROGRAM OBJECTIVES

The objective of the Read-Only Memories Program (NAS 5-10610), initiated on 13 March 1968 was to develop integrated complementary MOS read-only nonvolatile memories compatible with the read/write nondestructive readout volatile type memories developed through the Integrated Circuit Memory Program (NAS 5-10243). The read-only memories are provided as blank memories that can be easily programmed and have the capability of being programmed automatically. After programming the memory, data is to be basically indestructible. A new program requires a new blank memory. The memory is to nonvolatile; that is, neither the presence nor absence of the supply voltage should affect its memory content.

The fact that the read-only memory array must dissipate very little power in operation and in standby dictates that the approach be consistent with complementary MOS array technology. Also, since a small chip is required for maximum yields and minimum cost, the basic size of the array and thus the current carrying capability of the devices is limited. With these restrictions in mind three permanent nonvolatile memory techniques were studied during the course of the first phase of the Read-Only Memory Program. These three memory elements are the following: fusible interconnections, oxide breakthrough structures, and polarizable MNOS devices.

Typical characteristics desired for a ROM array using the memory elements developed in the first phase of the Read-Only Memory Program are:

a. Size - 16 words by 16 bits

b. Input - 4-bit address and read (1 = supply potential; 0 = ground potential)

Input resistance shall be greater than 1 megohm.

Input capacitance shall be less than 5 picofarads for each input line including the package capacitance.

c. Output - 16 preinserted data bits (1 = supply potential; 0 = ground potential)

Five microseconds after the simultaneous initiation of both the read pulse and address, the following shall have transpired:

(1) The output shall have driven a 30-picofarad load to within 90 percent of the supply voltage for an output change from 0 to 1.

(2) The output shall have driven a 30-picofarad load to within 10 percent of the supply voltage for an output change from 1 to 0.

If no read pulse is present all output lines are to be effectively open circuits.

d. Power - supply voltage 6 to 12 volts. Standby power dissipation at ambient - less than 0.01 milliwatt.

e. Input of data - data input by some method that permanently sets the information into the memory. The input must be capable of being easily accomplished in the laboratory and be capable of being made automatic.

f. Operating temperature range - -50 to +100°C.

2.2 FUSIBLE LINK MEMORY ELEMENTS

2.2.1 Introduction to Possible Fusing Mechanisms

Prior to the beginning of the Read-Only Memory Program, observations had determined that, when large currents were passed through thin aluminum films on silicon dioxide, it was possible to rupture the aluminum films. Further observations confirmed that the rupture of metal film resistors such as chromium or tantalum of high sheet resistivity, occurred very rapidly even at moderate current levels. Furthermore, it was found that aluminum interconnections failed when operated at moderate current levels for extended periods of time.

From this experience and from a study of metallurgical systems, it is seen that the rupture of thin metal films is likely to be caused by one or more combinations of several different physical mechanisms. Several possible mechanisms involved are:

a. vaporization caused by joule heating

b. partial solid solutions and diffusion caused by joule heating

c. oxidation caused by joule heating in an oxidizing atmosphere

d. electromigration caused by large current densities and accelerated by joule heating

e. solid-phase change caused by joule heating

f. mechanical rupture caused by differences in thermal expansion coefficients

g. thin film grain size and grain boundary changes caused by gas ambient and thermal conditions

h. order-disorder transformation.

Theoretical aspects of some of these possible mechanisms are discussed further in the following sections.

2.2.2 Thermal Considerations

Since the fusing mechanisms are so dependent on the temperature, considerable effort is given to the thermal conditions in the following paragraphs.

2.2.2.1 Heat Conduction Models of the Fusible Links

The fusible link is composed of a thin metal film with thicker contact electrodes on insulating film such as silicon dioxide. A one-dimensional heat flow model of the fusible link may be used if the following assumptions are made.

a. The power dissipated in the metal film is uniformly distributed so that no temperature gradients exist in the metal.

b. The heat conduction through the air (H_{AIR}) and through the metal contacts (H_{MC}) is negligible.

c. The radiated heat H_R is negligible.

d. The heat required to raise the volume of metal to temperature ($\Delta H_C = C_p \Delta T$) is negligible.

e. The insulating film is to be bounded by two planes such that the region $0 < z < z_{OX}$ is considered.

f. The temperature at the plane $z = 0$ is held constant at the initial temperature T_O.

g. A constant rate of heat transfer (q = joules/sec - cm^2) per unit area enters the surface at $z = z_{ox}$. Assumption (g) has been shown to be a valid assumption for similar cases such as a flat heating element on an insulator and for heat generated by surface friction. [1]

h. The specific heat (c_p) and thermal conductivity (k) are constant over the temperature range.

The physical heat flow model is shown in figure 1. Verification of these assumptions is discussed in a following section where the calculations are treated. It is important to note that as a result of the above assumptions the rate of heat transferred at the surface q_A ($z = 0$) is set equal to the power dissipated in the metal film (P_A).

The following paragraphs follow the development of the heat transfer rate and temperature as a function of distance (z) and time according to Carslaw and Jaeger. [2]

---

1. H. S. Carslaw and J. C. Jaeger, Conduction of Heat in Solids, (Oxford: Oxford Press, 1959), 75.
2. Carslaw and Jaeger, 75-78.

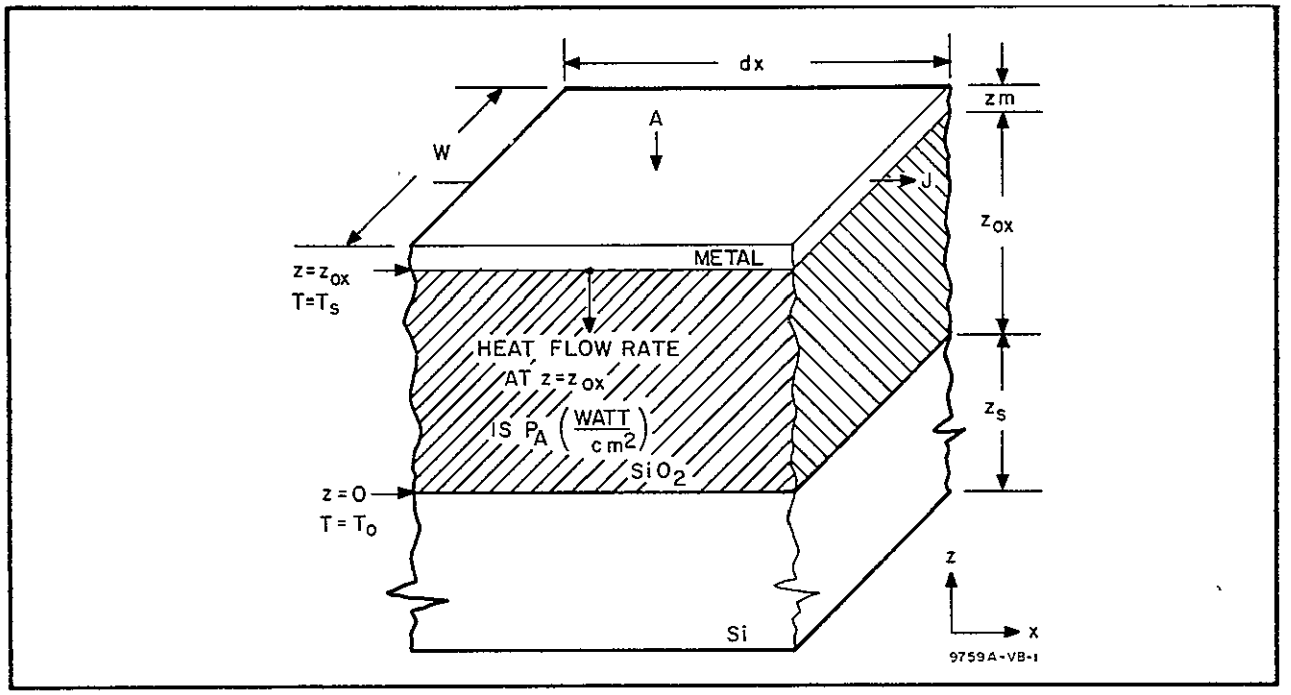

Figure 1. Heat Flow Model

The following terms are used in the development

q_A = flux of thermal energy ($\frac{\text{joules}}{\text{sec - cm}^2} = \frac{\text{watts}}{\text{cm}^2}$)

q = rate of heat transfer ($\frac{\text{joules}}{\text{sec}}$ = watts)

Q = heat energy (joules = watt - sec)

k = thermal conductivity ($\frac{\text{joules}}{\text{sec -cm°C}} = \frac{\text{watts}}{\text{cm -°C}}$)

K = thermal conductance (watts/°C)

ρ = density (gm/cm^3)

c_p = specific heat (joules/gm - °C)

C_p = volumetric specific heat = $\rho\, c_p$ ($\frac{\text{joules}}{\text{cm}^3\text{ -°C}}$)

α = thermal diffusivity = $\frac{k}{C_p}$ ($\frac{\text{cm}^2}{\text{sec}}$)

z = distance into the insulator (cm) measured from the surface where $T = T_o$

z_{ox} = thickness of the oxide insulating layer

t = time (sec)

T = temperature (°K)

T_o = initial temperature

A = surface area normal to the heat flow (cm^2)

P_A = power dissipated in resistor film per unit area

P = total power dissipated in the film

R_T = thermal resistance = $\frac{z_{ox}}{kA}$ ($\frac{\text{°C}}{\text{watt}}$)

The rate of heat transfer per unit area in a solid (heat flux) is given by

$$q_A = \frac{q}{A} = -k \frac{\partial T}{\partial z} \quad \frac{\text{joules}}{\text{sec - cm}^2} \tag{1}$$

and it satisfies the differential equation

$$\alpha \frac{\partial^2 q}{\partial z^2} = \frac{\partial q}{\partial t} \quad , \; z > 0, \; t > 0 \tag{2}$$

The solution of equation 2 for q_A with P_A = constant $(\frac{\text{watts}}{\text{cm}^2})$

$$\text{at } z = z_{ox}, \; t > 0 \text{ is } q_A = P_A \operatorname{erfc} \frac{z_{ox} - z}{2\sqrt{\alpha t}} \tag{3}$$

Thus from 1

$$-T_o = \int_z^\infty \frac{q_A}{k} \, dz \tag{4}$$

and from 3

$$T - T_o = \frac{P_A}{k} \int_z^\infty \operatorname{erfc} \frac{z_{ox} - z}{2\sqrt{\alpha t}} \, dz \tag{5}$$

$$\equiv \frac{2 P_A \sqrt{\alpha t}}{k} \operatorname{ierfc} \frac{z_{ox} - z}{2\sqrt{\alpha t}} \tag{6}$$

$$T - T_o = \frac{2 P_A}{k} \left\{ \left(\frac{\alpha t}{\pi} \right)^{1/2} \exp \left[\frac{-(z_{ox} - z)^2}{4 \alpha t} \right] \right.$$
$$\left. \frac{(z_{ox} - z)}{2} \operatorname{erfc} \frac{z_{ox} - z}{2\sqrt{\alpha t}} \right\} \tag{7}$$

The temperature at the surface where $z = z_{ox}$ is

$$T_s = \frac{2 P_A}{k} \left(\frac{\alpha t}{\pi} \right)^{1/2} + T_o \tag{8}$$

These equations hold for the conditions where the thickness of the film $z_{ox} > 2 \sqrt{\alpha t}$. The case where z_{ox} is not limited to a very thick film has also been considered by Carslaw and Jaeger. Their solution[3] for this case which is directly applicable is

---

3. Carslaw and Jaeger, op. cit., 113.

$$T - T_o = \frac{P_A z}{k} - \frac{8 P_A z_{ox}}{k \pi^2} \sum_{n=o}^{\infty} \frac{(-1)^n}{(2n+1)^2}$$

$$\exp - \left[\frac{\alpha (2n+1)^2 \pi^2 t}{4 z_{ox}^2} \right] \sin \frac{(2n+1) \pi z}{2 z_{ox}} \qquad (9)$$

A good approximate solution is given by the n = 0 term of the above expression. Also if a time constant τ is defined as

$$\tau = \frac{4 z_{ox}}{\alpha \pi^2} \qquad (10)$$

the simplified expression becomes

$$T(z, t) - T_o = \frac{P_A z}{k} - \frac{P_A z_{ox}}{k} \exp - \left(\frac{t}{\tau}\right) \sin \frac{\pi z}{2 z_{ox}} \qquad (11)$$

and the temperature at the surface T_s where $Z = Z_{ox}$ is

$$T_s = \frac{P_A z_{ox}}{k} \left[1 - \exp - \left(\frac{t}{\tau}\right)\right] + T_o \qquad (12)$$

For $t > \tau$, equation 11 reduces to the familiar equation

$$\Delta T = \frac{(P_A \quad A)\ \Delta z}{kA} = P R_T \qquad (13)$$

which is the case for steady state heat transfer.

The total amount of heat Q transferred is

$$Q = \int_o^t q(t)\, dt \qquad (14)$$

Since the rate of heat transfer is a constant (P_A) for the above models, the total heat supplied and transferred per unit area is

$$Q_A = P_A t \qquad (15)$$

and the total heat supplied and transferred is

$$Q = P \cdot t \qquad (16)$$

2. 2. 2. 2 Calculations to Justify the Model

Since the thermal calculations are dependent on the various constants of the materials involved, the constants are given for T = 300°K in table 1. Where the temperature excursions become large, the temperature dependence must also be taken into account. The high temperature conditions are detailed in a following paragraph.

The first calculation will be the time constant τ and equilibrium temperature for a typical fusible link geometry.

Let P = 0.1 W

A = 10 by 100 micrometers (0.4 x 4 mils)

$= 10^{-5}$ cm^2

therefore

$$P_A = 10^4 \frac{\text{joules}}{\text{sec - cm}^2}$$

for SiO_2 $k = 0.014$ watt/cm - °C

$\alpha = 0.006$ cm^2/sec

$z_{ox} = 10^{-4}$ cm (10,000 Å)

Therefore, in equilibrium the surface temperature from equation 12

$$T_S = \frac{P_A \, z_{ox}}{k} + T_o$$

$$= \frac{(10^4)\ (10^{-4})}{0.014} + 30°C$$

$= 100°C$ at P = 0.1 W

and

$T_s = 730°C$ at P = 1.0W

The time constant gives the time at which the temperature is about 63 percent of the equilibrium temperature and is

$$\tau_{SiO_2} \cong \frac{0.4\ (10^{-8})}{0.006} = 0.66\ \mu\text{sec.}$$

TABLE 1

THERMAL CONSTANTS (T = 300 °K)*

	Symbol.	Units	Si	SiO_2	Al	Cr	Ti	Pt
Density	ρ	gm/cm^3	2.33	2.27	2.7	7.2	4.54	21.5
Thermal Conductivity	k	$\frac{watt}{cm\ °C}$	1.5	0.14	2.37	0.87	0.20	0.69
Specific Heat	c_p	$\frac{joules}{gm-°C}$	0.71	1.0	0.9	0.45	0.52	0.133
Volumetric Specific Heat	C_p	$\frac{joules}{cm^3-°C}$	1.63	2.27	2.42	3.22	2.36	2.85
Thermal Diffusivity $\frac{k}{C_p}$	α	$\frac{cm^2}{sec}$	0.92	0.006	0.98	0.27	0.085	0.241

* Dwight B. Gray, ed., American Institute of Physics Handbook (New York: McGraw-Hill, 1963), 4-77 to 4-100, 4-47 to 4-52.

9759A-VA-2

The rate that energy must be supplied per unit area to raise the temperature of a metal film of thickness z_M (0.1 micrometer) is

$$q_A = \frac{d Q_A}{dt} = C_p \, z_M \, \frac{dT}{dt} \tag{17}$$

This may be calculated from the constants and

$$\frac{dT}{dt} = \frac{\Delta T}{\Delta t} = \frac{0.63 \, (T_s)}{6.6 \times 10^{-7} \text{ sec}} \simeq \frac{10^8 \text{ deg}}{\text{sec}} \tag{18}$$

$$\cong 10^8 \text{ deg/sec at } P_A = 0.1 \text{ watt}$$

$$= 10^9 \text{ deg/sec at } P_A = 1.0 \text{ watt}$$

which is the approximate rate at which the temperature increases during the transient state. Therefore, for aluminum which has the largest specific heat of the metals considered, the rate of heat that must be supplied is

$$q_A = (2.42) \, (10^{-5}) \, (10^8) \tag{19}$$

$$= 2.42 \times 10^3 \ \frac{\text{watts}}{\text{cm}^2} \text{ at } P_A = 0.1 \text{ watt}$$

and

$$q_A = 2.42 \times 10^4 \ \frac{\text{watts}}{\text{cm}^2} \text{ at } P_A = 1.0 \text{ watt}$$

Since the heat is actually being supplied at a rate

$$q_A = 10^4 \ \frac{\text{joules}}{\text{sec - cm}^2} \text{ at } P_A = 0.1 \text{ watt}$$

the rate at which heat is being used to raise the metal temperature may be neglected and assumption (d) is justified.

Assumption (a) is justified because of the great difference in thermal conductivity between the metal and the oxide. Assumption (b) (H_{AIR} neglected) is justified because the thermal conductivity of air is about $2.6 \times 10^{-4} \ \frac{\text{watt}}{\text{cm - °C}}$ which is two orders of magnitude smaller than the insulator. Furthermore,

the cross-sectional area of the metal film normal to the x direction is typically several orders of magnitude less than in the z direction, and thus H_{MC} may also be neglected. Assumption (f) which states that there is a negligible increase at the silicon-silicon dioxide interface may also be justified. The time constant to reach the equilibrium temperature at the silicon surface, if a constant rate of heat P_A is supplied and the silicon is 10 mils thick, is from equation 10

$$= \frac{0.4\ (250 \times 10^{-2})}{0.97} = 0.23 \text{ msec.} \qquad (20)$$

Since most of the measurements were made with pulsewidth of less than 0.1 msec, it can be seen from equation 12 that the temperature increase at the silicon surface was negligible. Even under equilibrium conditions the temperature at the surface is probably negligible since the linear heat flow model for the silicon is no longer valid. The result is a much greater effective cross-sectional area, and this, combined with the larger thermal conductivity, gives a low silicon thermal resistance in equilibrium.

Another ramification of the long thermal time constant of the silicon is that it seems practically impossible to sense the rapid increase in temperature over a small area on the surface of the silicon dioxide using junctions in the silicon.

2.2.2.3 Thermal Runaway and Metal Volatilization

Thermal runaway may be described generally as an unstable process by which a temperature increase causes an increase in the rate of heat generation per unit area (P_A) which in turn causes an increase in temperature to the point where destruction or change of the metal film occurs to limit the process. As discussed in paragraph 2.2.1, there are several possible changes that can occur in the metal film; however, only the extreme high temperature case of metal volatilization will be discussed in this paragraph.

The first consideration is the description of hotspot development in a metal film. If a constant current (typical of MOSFET switches) is applied to an essentially homogeneous resistor film that has a uniform resistance per unit length, the power dissipated per unit area in the film will be uniform, and the temperature increase in the film will also be uniform except for the second order effect of heat loss through the contacts to the film. This idealized condition is shown in figure 2A. However, if a nonuniformity in the film exists such as a nonuniform cross section or a nonuniform resistivity, the conditions are established for thermal runaway. Figure 2B shows that if the pulsed, constant-current source is applied to the nonuniform resistor film, the temperature increase caused by the large power per unit area dissipated will additionally cause an increase in resistance followed by a further increase in the temperature. The metal films considered had positive temperature resistance coefficients. Also at the high temperatures experienced, several of the mechanisms mentioned previously can contribute to the increase in resistance per unit length further enhancing the runaway condition. For example, the formation of a binary alloy will increase the resistivity; physical strain will increase the resistivity; [4] and electromigration can decrease the cross-sectional area.

The problem is to determine the temperature and the amount of heat per unit area that is required to volatilize the metal at the hotspot. Secondly, it must be determined that this amount of heat per unit area is possible to attain; given the linear heat flow model of paragraph 2. 2. 2. 2.

---

4. E. Condon and H. Odishaw, ed., Handbook of Physics (New York: McGraw-Hill 1967), 4-74, 4-78.

The heat required to change the temperature and achieve change of phase may be calculated by taking into account the heat capacitance (C_p) change, at constant pressure, with temperature and the latent heat of fusion and vaporization. Equations derived empirically[5] and typical constants listed in table 2 are used for the calculations. The heat capacitance is

$$C_p = a + (b \times 10^{-3})\, T + (C \times 10^{-6})\, T^2 + \frac{d \times 10^{-5}}{T^2} \tag{21}$$

The heat content is

$$H_T - H_{298} = \int_{298}^{T} C_p \, dT \tag{22}$$

$$= a\,T + 1/2\,(b \times 10^{-3})\, T^2 + 1/3\,(C \times 10^{-6})\, T^3 - \frac{d \times 10^{-5}}{T} - A \tag{23}$$

The heat content is given by a sum of terms for each phase of the substance involved in the temperature range considered plus terms which represent the heats of transitions (ΔH_{TR}).

$$H_T - H_{298} = \Sigma \int_{298}^{T} c_p \, dT + \Sigma \Delta H_{TR} \tag{24}$$

The heat energy required per unit of surface area to volatilize a metal strip of thickness z_m is

$$H_A = z_m \Sigma Q_\nu \tag{25}$$

If the metal film is 1000 angstroms thick (z_m = 0.1 micrometer) the volatization heat required per unit area is

$$H_A\,(z_m = 0.1 \text{ micrometer}) = \Sigma Q_\nu \; 10^5 \; \frac{\text{joules}}{\text{cm}^2} \tag{26}$$

---

5. Robert C. West, ed., Handbook of Chemistry and Physics: Thermodynamic Properties of Elements and Oxides, Ed. 49 (The Chemical Rubber Co., Cleveland, Ohio, 1968), D-32-D-37.

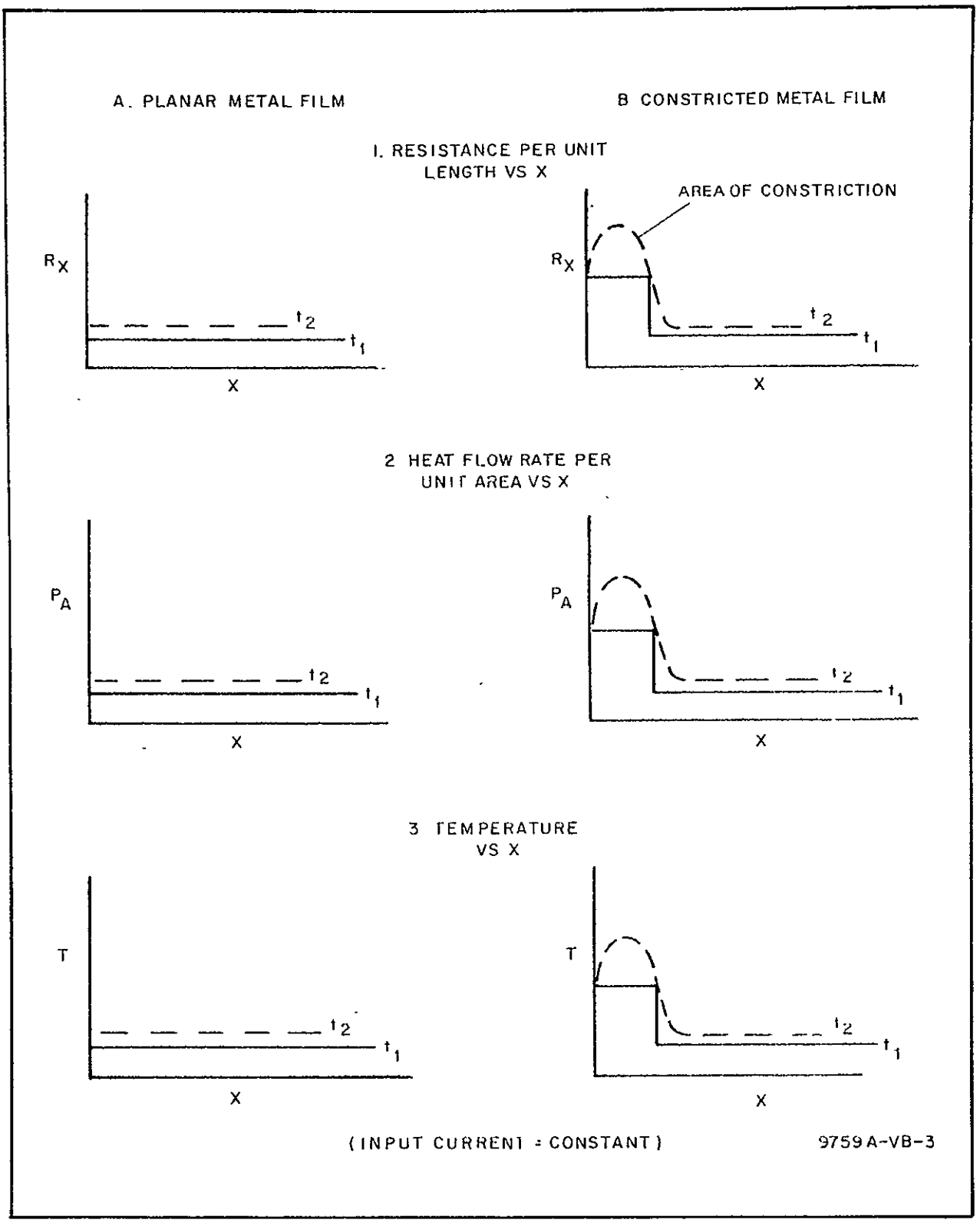

Figure 2. Resistance, Power Density, and Temperature in Constricted Metal Films as Compared to a Planar Film at Time t_1 and t_2

TABLE 2

THERMODYNAMIC PROPERTIES OF ELEMENTS AND OXIDES

Solid	Process	Phase		Transition Temperature (°K)	Heat of Transition (K cal/mole)
		Initial	Final		
Al	Fusion	solid	liquid	933	2.57
	Vapor	liquid	gas	2,600	67.9
Al_2O_3	Fusion	solid	liquid	2,300	(26)
Cr_2	Fusion	solid	liquid	2,173	3.5
	Vapor	liquid	gas	2,495	72.97
Cr_2O_3	Fusion	solid	liquid	2,538	(25)
CrO_2	Decomposition			700	
CrO_3	Fusion	solid	liquid	460	(6.1)
	Vapor	liquid	gas	(1,000)	(25)
Pt	Fusion	solid	liquid	2,042	5.2
Si	Fusion	solid	liquid	1,683	11.1
	Vapor	liquid	gas	2,750	(71)
SiO_2	Trans	solid β	solid α	856	0.15
	Fusion	solid β	liquid	1,883	2.04
	Decomposition			2,250	
Ti	Trans	solid α	solid β	1,155	0.95
	Fusion	solid	liquid	2,000	(4.6)
	Vapor	liquid	gas	3,550	(101)
TiO	Trans	solid α	solid β	1,264	0.82
	Decomposition			2,010	
Ti_2O_3	Trans	solid α	solid β	473	0.215
	Fusion	solid β	liq	2,400	(24)
	Vapor	liq	gas	3,300	
Ti_3O_5	Trans	solid α	solid β	450	2.24
	Fusion	solid β	liq	2,450	
TiO_2	Fusion	solid	liq	2,128	(16)
	Decomposition			3,200	

9759A-TB-4

The condition necessary to volatilize a metal film situated on an insulator, as in the model previously discussed, is that the heat energy supplied must be sufficient to supply both the heat lost by conduction and the heat required to volatilize the metal. An estimate of the metal film size and input power levels for which volatilization is possible can be calculated using the model previously discussed and the information in table 2. The conditions and summary of the calculations are detailed in the following paragraph for a typical aluminum fusible link.

The conditions are the following:

a. z_{ox} = 1 micrometer

b. $z_{ox}/k = 7 \times 10^{-3} \frac{°C - cm^2}{watt}$

c. τ = 0.66 μsec, 3 τ = 20 μsec

d. metal film width = 10 micrometers (0.4 mil)

metal film thickness = 0.1 micrometer

metal film length = x

e. ΣQ_ν (aluminum) $\equiv 3.9 \times 10^4$ joules/cm^3

H_A (aluminum) = 0.39 joule/cm^2

volatilization temperature T_ν = 2,870°C

f. input power density required to reach T = 2,870 is

$P_A = 4.1 \cdot 10^5 \frac{watts}{cm^2}$ (heat lost by conduction)

input energy density at T = 2,870 (t = 3τ) is Q_A (3τ) = 0.82 joules/cm^2.

The total energy required to bring the metal film up to temperature and volatilization is about 1.2 joules/cm^2. Since the rate at which the energy must be supplied to volatilize the film is unknown, it is difficult to estimate the power density required. The energy density required to volatilize, however, is still much less then the energy required to reach the temperature of volatilization.

For estimation purposes it will be assumed that the 0.39 joules/cm^2 required for vaporization, is supplied in 10^{-6} sec. The power density then is 3.9×10^5 watts/cm^2.

The total power density required then to raise the temperature of the system and volatilize the metal is about 10^6 watts/cm^2. If the power is dissipated in only 1 micrometer of length in a nonuniform film, the power required is 0.1 watt. The power required for a 10 micrometer (0.4 mil) length is 1 watt. The conclusion is that the temperature of volatilization can be reached with these power levels.

2.2.3 Electromigration

Considerable attention has been given to electromigration phenomena because many of our experimental observations can be explained by this effect. The theory of electromigration has been reviewed during the course of the program and a more general extension[6] of the theory is presented in the following paragraphs.

Recently, observations have appeared in the literature of the rupture of aluminum due to the transport of material under high current densities of the order of 10^6 A/cm^2 where open interconnects have occurred after periods of several hundreds of hours. Attempts have been made to correlate this data in terms of physical phenomena, meantime-to-failure, current densities, and temperature by Black[7] and Blech and Sello.[8] Previous investigations of

---

6. D.D. O'Sullivan, "Electromigration in Aluminum and Chromium Metal Films," Defense and Space Center Technical Memo, D.S.C. 7796, (1969).
7. J.R. Black, "Metallization Failures in Integrated Circuits," "Technical Report No. RADC - TR - 67- 477," (September 1967).
8. I.A. Blech and H. Sello, "The Failure of Thin Aluminum Current - Carrying Strips on Oxidized Silicon," Physics of Failure in Electronics, V, (1967), 496-505.

material transport at high current densities have been conducted by R. V. Penny,[9] and by H. B. Huntington,[10] A. R. Grove,[11] and P. S. Ho[12] using wires. Two phenomena manifest themselves in these investigations. One is electromigration, and the other is the Soret effect.

Although the Soret effect is not explicitly a part of the problem with which we are concerned, namely electromigration, the observation does relate to this discussion and will be mentioned briefly.

The Soret effect is the migration of material down a thermal gradient and can go on simultaneously with electromigration. With the exception of cobalt, the Soret effect is not a dominating mechanism for the migration of material. The migration due to the Soret effect can be correlated with the temperature distribution in the wire observed and is readily separable from electromigration. In gold, aluminum, and copper the primary mechanism is that of electromigration for the transport of material. The data, collected by initial investigators, was the result of experiments conducted on wires with high current densities flowing through them and the observation of the motion of material as a function of time and temperature. Huntington, Fiks,[13] and Bosvieux and Friedel[14] have set forth the explanation of this phenomenon in

---

9. R. V. Penny, "Current Induced Mass Transport in Aluminum," J Phys Chem Solids, XXV, (1964), 334-335.
10. H. B. Huntington and A. R. Gove, "Current Induced Marker Motion in Gold Wires," J Phys Chem Solids, XX, (1961), 76-87.
11. A. R. Grove, "Current-Induced Marker Motion in Copper," J Phys Chem Solids, XX, (1961), 88-93.
12. P. S. Ho and H. B. Huntington, "Electromigration and Void Observation in Silver," J Phys Chem Solids, XXVII, (1966), 1319-1322.
13. V. B. Fiks, "On the Mechanism of the Mobility of Ions in Metals," Sov Phys Solid State, I, (1964), 14-28.
14. C. Bosvieux and J. Friedel, "Sur L' Electrolyse Des Alliages Metalliques," J Phys Chem Solids, XXIII, (1962), 123.

terms of momentum exchange between the electrons flowing in the wire and the ions contained therein, under an applied electrical field. This approach explains the difference in the direction of motion of markers on the wire at high current densities. This discussion applies to direct current as opposed to alternating current flowing in the wire. Blech and Sello noted similar phenomena in the case of thin metal interconnects on integrated circuits and have published data summarizing these results. In particular, they have been able to establish a systematic relationship between meantime-to-failure (MTF), current density, and temperature.

Since the phenomena of metal transport and depletion can be carried out in a controlled manner with the purpose of interrupting the flow of current in the metal, the term meantime-to-failure is inappropriate. This time will be defined for our purposes as the time to interrupt the current and will be symbolized as τ_I. Black, using a heuristic argument, derived the relationship:

$$\frac{1}{(\tau_I)\, J^2} = Ae^{\frac{-\phi}{kT}} \tag{27}$$

between the aforementioned variables. Equation 27 is an Arrhenius type relation when:

τ_I = the time to current interruption

J = the current density

ϕ = the activation energy

A = an appropriate constant

k = Boltzmann's constant

T = the temperature in degrees Kelvin.

The argument is as follows:

a. The electric field applied to the conductor will exert a force on the activated ions in the direction opposite to electron flow.

b. The rate of momentum exchange between the conducting electrons colliding with the activated metal ions will exert a force on the metal ions in the direction of electron flow.

The rate of reaction is then expressed as:

R = F (electron momentum) × (number of striking electrons) × (effective target cross section) × (target density)

where F is an appropriate constant. The additional momentum gained by an electron accelerated by an electric field a distance of its mean free path l, with an average velocity, v, is:

$$\Delta P = \frac{eEl}{v} = e\rho J \frac{l}{v} = e\rho J \bar{\tau} \tag{28}$$

where

ρ = the resistivity

τ = the mean free time between collisions

e = the charge on an electron.

The number of electrons arriving per unit time, in a square centimeter is:

$$n = \frac{J}{e} \tag{29}$$

The target density is given by an Arrhenius equation as a function of temperature by:

$$\text{Target density} = F_1 e^{-\phi/kT} \tag{30}$$

where F_1 is an appropriate constant.

The current interruption time (τ_I) then is related to the rate of mass transfer by:

$$\frac{F_2}{\tau_I} = R \tag{31}$$

where F_2 is an appropriate constant. Therefore, it is possible to write for the rate of reaction:

$$R = \frac{F_2}{\tau_I} = \left(\frac{e\rho J \ell}{V}\right) \frac{J}{e} \sigma \left(F_1 e^{-\frac{\phi}{kT}}\right) = \left(\frac{\rho l}{v} \sigma J^2\right) \left(F_1 e^{-\frac{\phi}{kT}}\right) \tag{32}$$

where σ is the target cross section. Simplifying by collecting constants

$$\frac{1}{\tau_I} = AJ^2 e^{-\frac{\phi}{kT}} \tag{33}$$

where A is an appropriate constant.

Taking the logarithm of both sides of equation 33:

$$\ell n\ (\tau_I) = -2\ell nJ + \left(\frac{\phi}{kT} - \ell nA\right) \tag{34}$$

As a result of this analysis it is expected that a plot of $\ell n\ \tau_I$ vs ℓnJ should be linear and have a slope of -2 and an intercept which varies with temperature as 1/T.

In most of the previous data taken by Black as well as Blech and Sello the τ_I was on the order of hundreds of hours. The current densities were on the order of 10^6 A/cm^2, and temperatures were above 100°C.

Using the above cited relation, a comparison was attempted in this laboratory. The results are summarized in the figures which follow. The data was obtained for aluminum and chromium since these materials are commonly used for interconnections in integrated circuits and thin film resistors respectively. At this point, certain remarks are in order.

a. The data obtained is limited and is by no means exhaustive.

b. Qualitatively our data and those of others are consistent.

c. The slope of -2 should be in fact temperature dependent.

d. A linear relationship of the form

$$\ell n\tau_I = -\alpha\ (T)\ \ell nJ + \beta\ (T) \tag{35}$$

exists between ℓnJ and $\ell n\tau_I$.

e. Preliminary results indicate that both α (T) and β (T) are linear functions of 1/T.

A plot of $\ell n\tau_I$ vs ℓnJ for an ideal fusible link material is shown in figure 3.

Note that for the ideal material the fusing current threshold is 10^6 A/cm^2. When the current is below this threshold value, the lifetime of the element is infinite. For the typical nonideal situation such as aluminum, the threshold current is much higher, and the threshold is not as sharply defined.

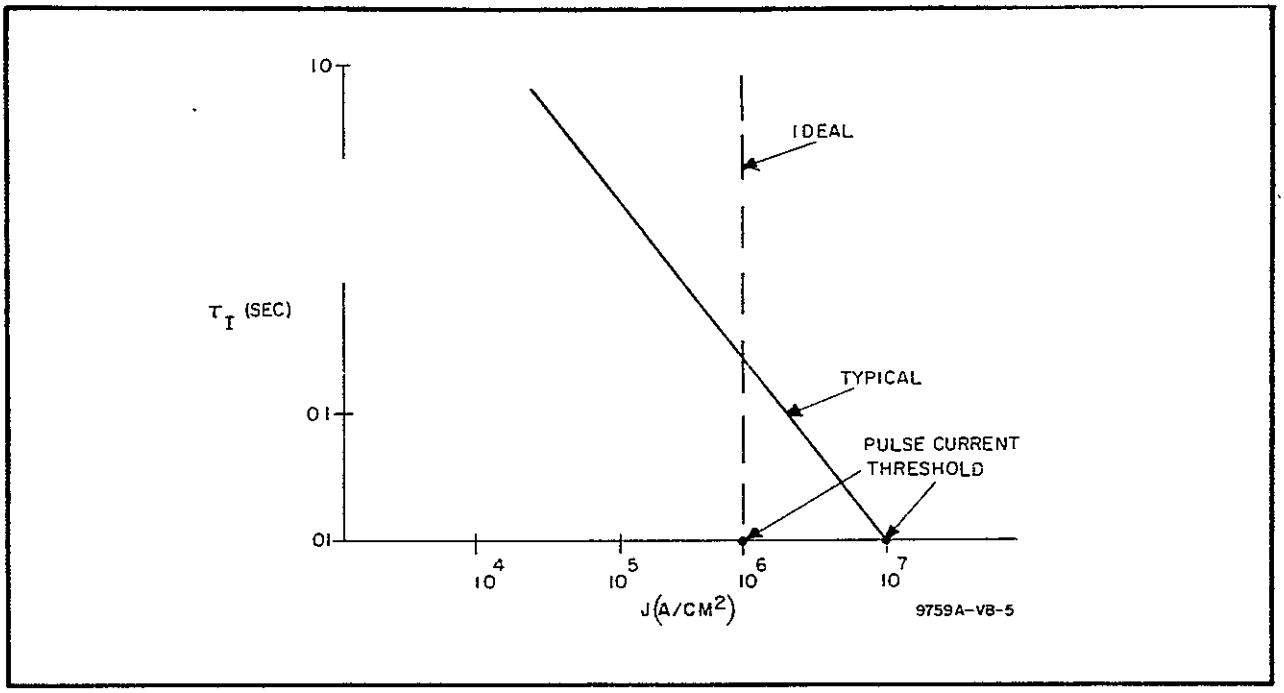

Figure 3. Interrupt Time (τ_I) vs Current Density(s)

The lifetime of an actual fuse element is finite and usually must be protected via current limiting devices to prevent undesired fusing.

2.2.4 Experimental Approach

At the beginning of this program the following factors were taken into consideration.

a. Since the fusible link must be ultimately incorporated into a low-power integrated circuit array, the processing used was made compatible with the processing of CMOS integrated circuit arrays.

b. Since the fusing current level was not of primary concern initially, the major effort was directed towards varying the processing parameters to minimize the current required on relatively large devices.

c. Methods of obtaining high reliability for the fusible link array were considered. Both the intrinsic device current threshold and circuit techniques to prevent undesired fusing were studied.

The various processing sequences considered may be placed in the following four categories which are shown in figures 4 through 7. There were also many processing variations. These variations involved the deposition parameters for chromium and aluminum and the subsequent heat treatments in various gas ambients. A detailed cross section of the constriction in the fusible link caused by partial shadowing of the deposition by the much thicker contact pod is shown in figure 8.

a. Same metal type for both contact pads and fusible link - planar fusible link (figure 4).

b. Same metal type for both contact pads and fusible link - fusible link with a built-in constriction in thickness (figure 5).

c. Different metal types for the contact pads and fusible link - planar fusible link (figure 6).

d. Different metal types for the contact pads and fusible link - fusible link with a built-in constriction in the thickness (figure 7).

Some additional processing parameters involved took into account the nature of the silicon dioxide surface on which the metal is deposited. For example, fusible links were evaluated on the phosphorus glass that is typical of the phosphorus passivation used for CMOS arrays.

The experimental observations were primarily monitoring of the film resistance, film thickness, the ohmic contact characteristics, and the voltage and current required to cause rupture of the fuse under various pulse type conditions. Some measurements were also taken under dc conditions for long periods to determine the relationship between the current density and the current interrupt time. Visual inspection and photographs of the fuses were made before and after the fusing. An attempt was also made to monitor temperature of the fuse under various conditions but without much success because of the short pulse times.

The requirements imposed by MOS transistor array considerations were taken into account in the measurement techniques. The conclusion is that a

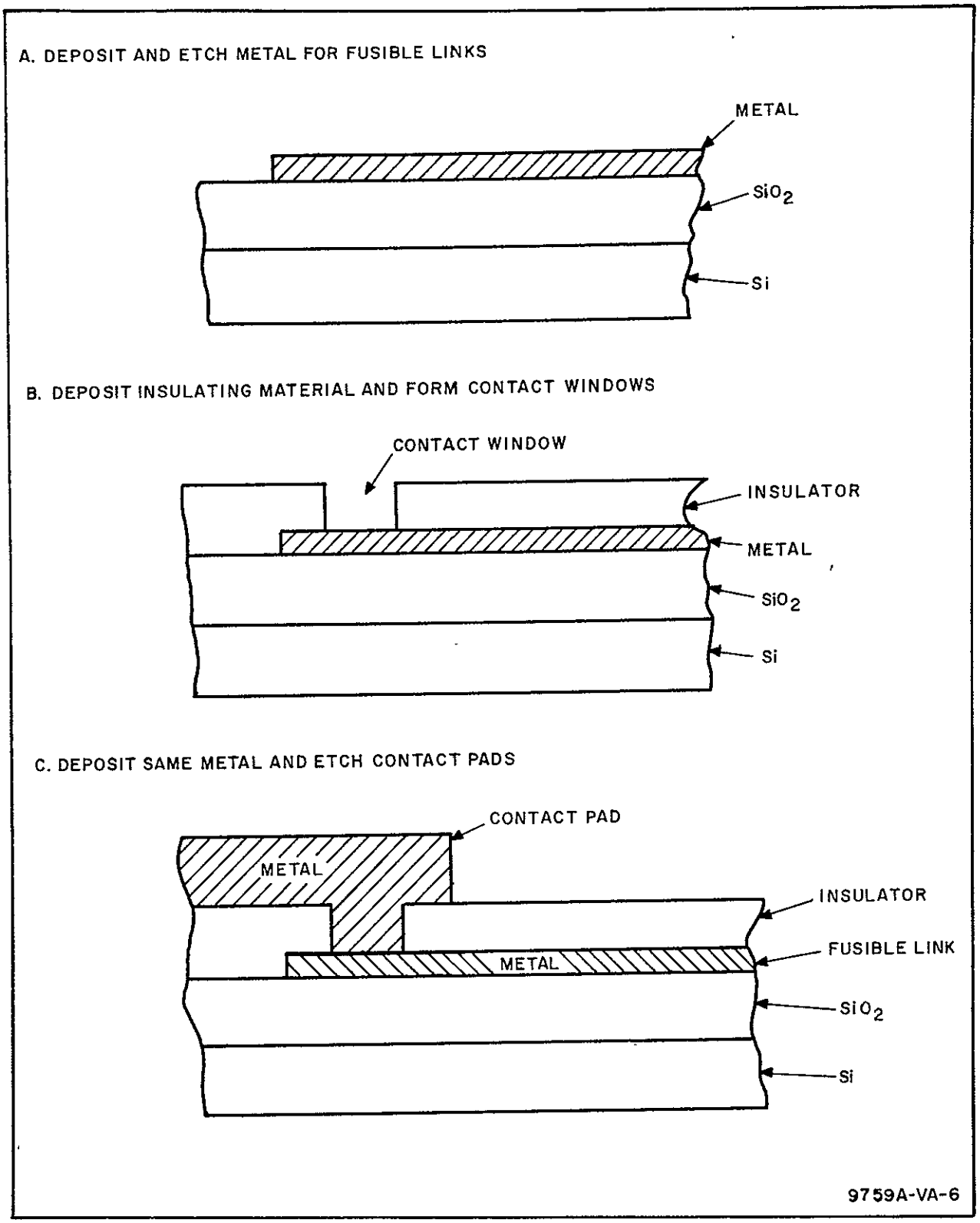

Figure 4. Planar Metal Film With Contact Pads of the Same Metal

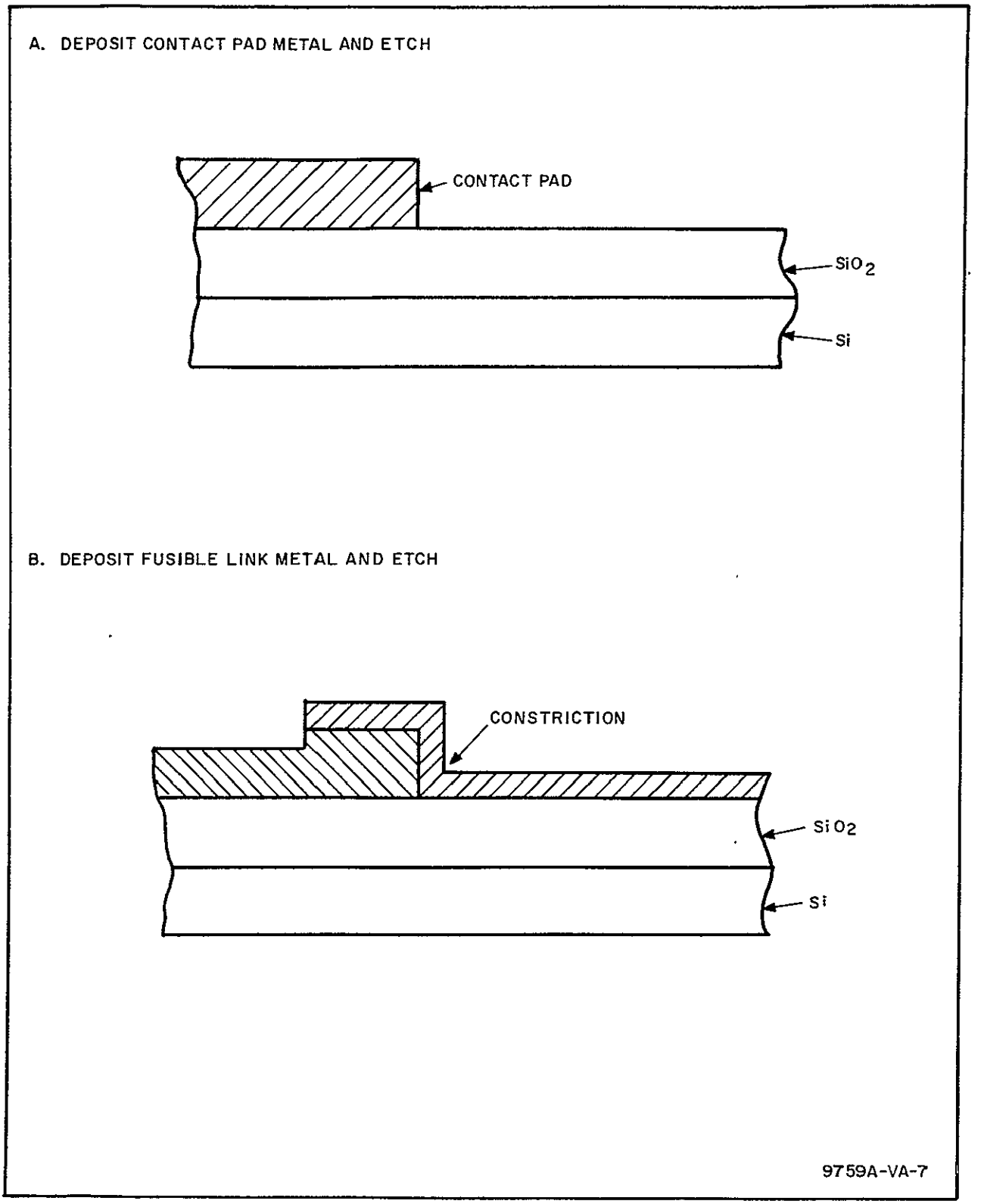

Figure 5. Constricted Fusible Link Formed Using Etching Technique (Same Metal)

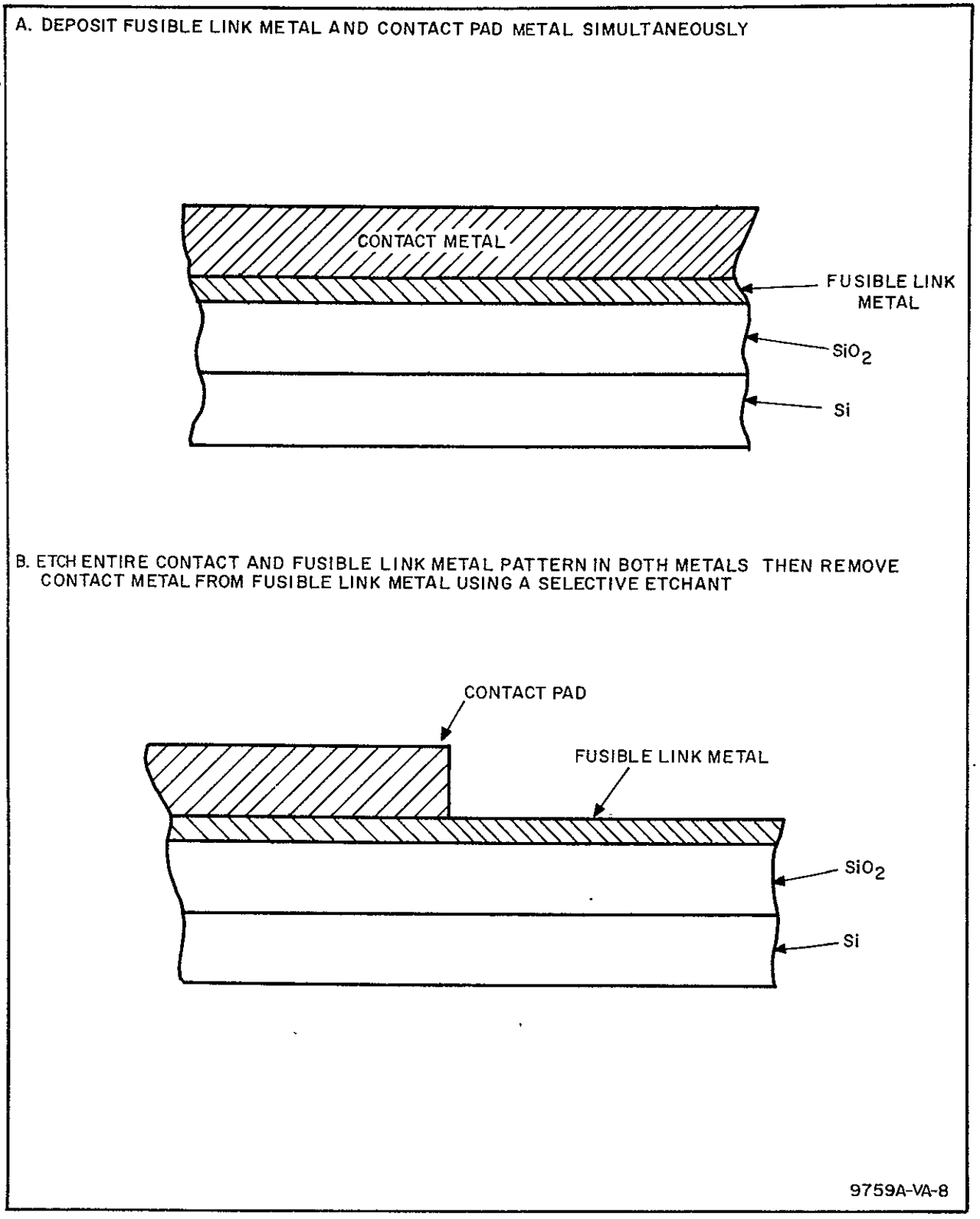

Figure 6. Planar Metal Film With Contact Pads of Different Metal

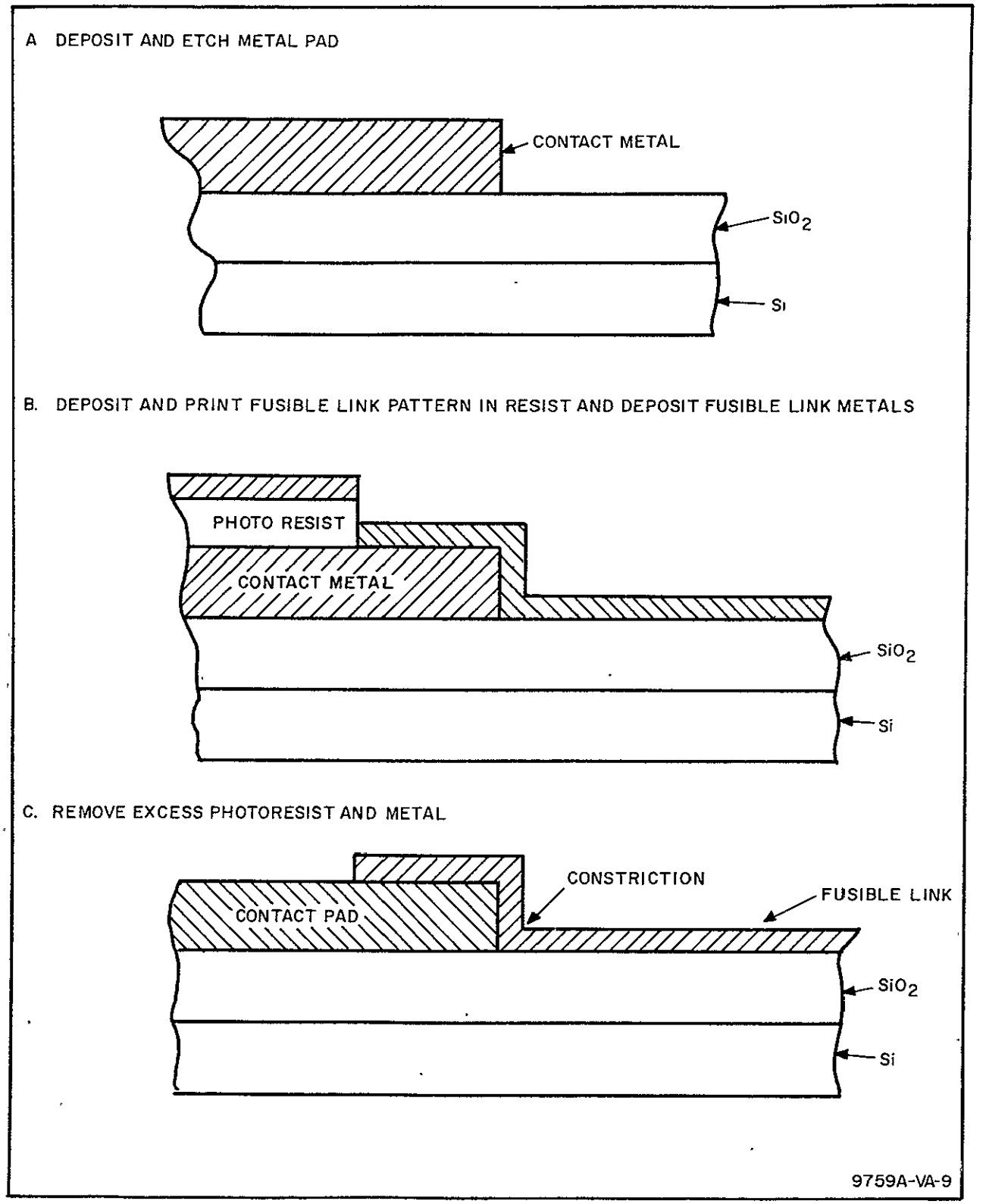

Figure 7. Constricted Fusible Link Using Photoresist Washout Technique (Different or Same Metal)

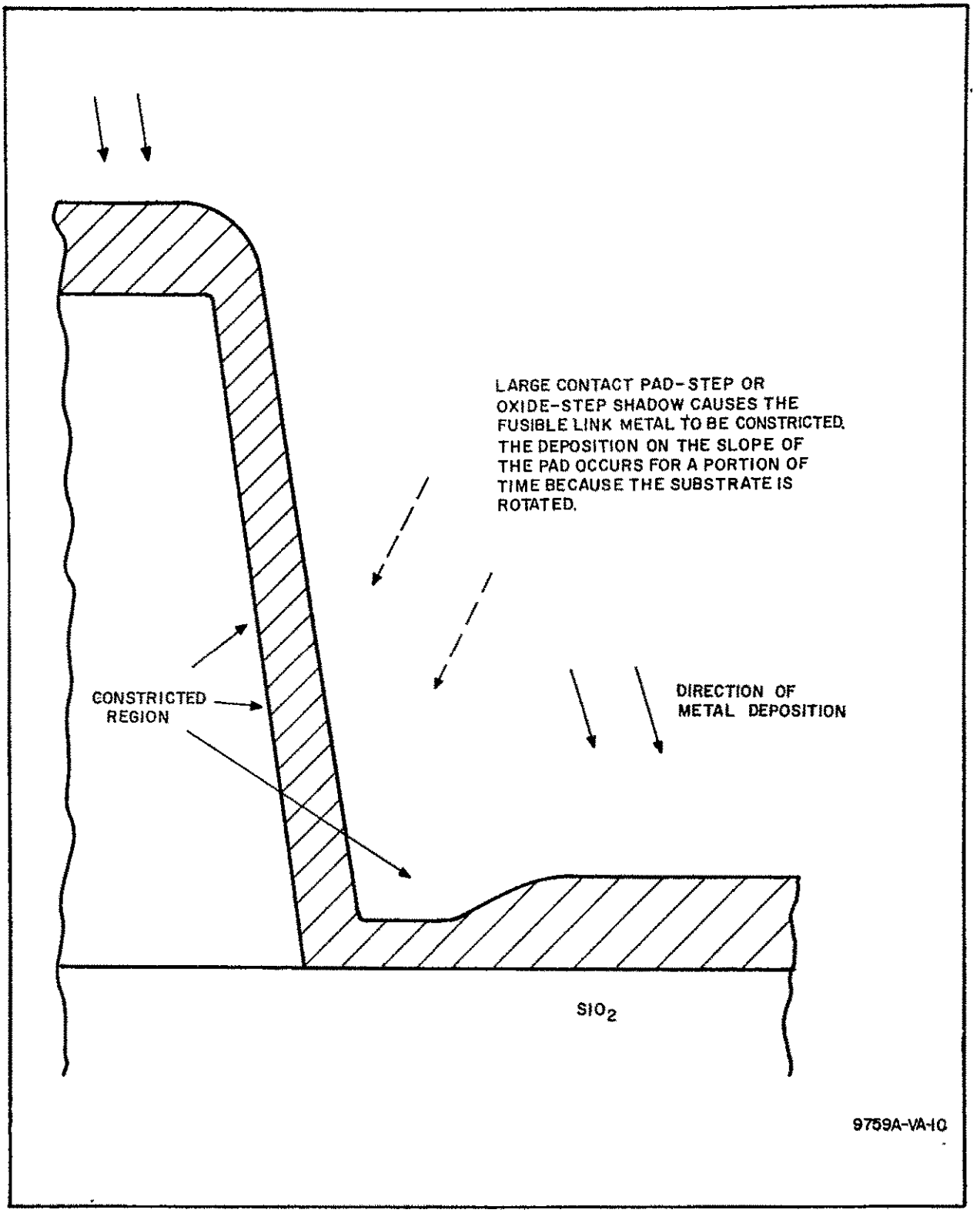

Figure 8. Detailed Cross Section of Constricted Fusible Link

voltage source with a 500-ohm source resistance would be representative of a typical MOS transistor in the array. All of the pulse tests were taken with a 500-ohm resistor in series with the pulse generator to simulate these MOSFET conditions. A pulse generator was utilized that had a single pulse capability and a very low duty cycle, multiple pulse capability. The rise-time and pulsewidth of the voltage source were variable. Voltages up to 50 volts were available from the voltage source, and currents as large as 100 milliamperes at that level were possible. The electrical test setup and the equations used for some of the electrical calculations are shown in figure 9.

2.2.5 Observations and Test Results

The most reliable and reproducible fusible link with low-current threshold (less than 10 mA) and current interruption times of less than 100 μsec have been the constricted chromium-chromium oxide films on aluminum contact pads. Most of the experiments, including life tests, were conducted on this

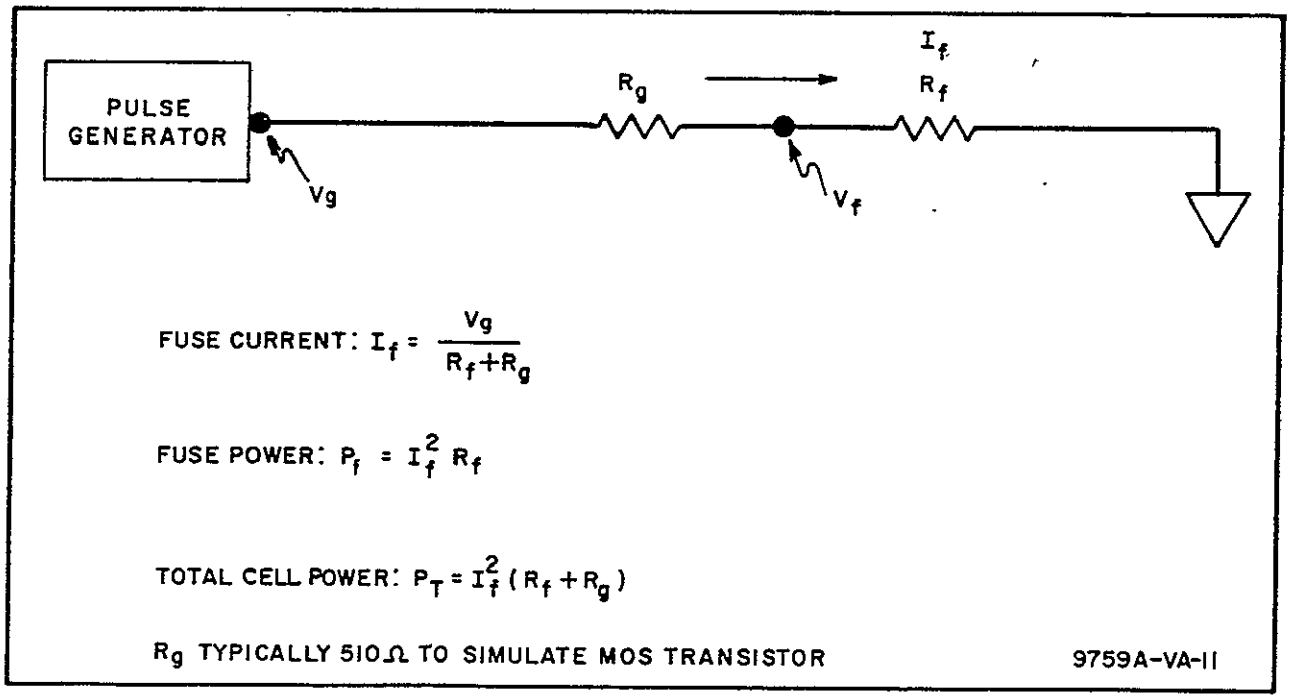

Figure 9. Electrical Test Setup

type of read-only memory elements. Other types investigated have been planar Cr films, planar Al films, and constricted Al films. It appears that with a reduction in area the planar Cr films can be made with sufficiently low-current threshold with even greater reproducibility.

2.2.5.1 Constricted Cr Films on Al Contact Pads.

A summary of the measurements and calculations for the constricted Cr fusible link on Al contact pads is shown in table 3, part A. The main variables were sheet resistivity, thickness, and the pattern definition process. The pattern definition process involves a washout technique where the Cr film was deposited on photoresist, and a second technique where the Cr is deposited and then chemically etched. Because of the presence of the photoresist for the washout technique, the vacuum deposition was not carried out at as low a vacuum pressure as for the etched Cr technique. It is believed that the lower vacuum pressure associated with the washout technique allows a greater proportion of the Cr film to be composed of Cr oxides. Since the Cr deposition rate in the shadow of the aluminum contact (the construction) is very slow, it is expected that the resistivity at the constriction is much higher as a result of the oxide formation. These factors contribute to the high resistance of the fusible links on wafers CX45, CZ32, and CX47 which is not consistent with the geometry and the sheet resistance measured during deposition. Furthermore, a contact voltage barrier existed. It was learned that sintering of the aluminum in N_2 prior to Cr deposition, in virtually every case, eliminated the contact voltage barrier V_B. In some cases, however, sintering after formation removed the barrier voltage.

The fusing current for representative elements as seen from table 3 is 10 mA total or 5 mA per branch. Photographs of representative elements fabricated using the washout technique are shown in figure 10. All of these elements were fused with a single voltage pulse as shown in table 3 of 100 μsec duration. Several interesting features are shown by the photographs which were taken with filtered light for emphasis. First, the change in the

Cr film color spreads from the cathode toward the anode. Second, an apparent void occurs at the constriction near the cathode. Third, the spreading of the Cr outside of the original pattern as in figure 10A is greatest for the lowest sheet resistivity (thickest) film. Fourth, the color change spread further for the highest sheet resistivity (thinnest) film (figure 10C), and fifth, it is seen in figure 10C that even though the anode does not make contact with the upper branch in a symmetrical fashion, the color change has spread from the cathode in a symmetrical manner.

The first two points support the theory of electromigration of Cr or Cr oxide ions from the cathode toward the anode. The third point indicates that high temperatures occur at the cathode, and the temperature reached is sufficient for fusion of Cr oxides. The molten Cr oxides either diffuse or migrate along the temperature gradient. It is seen in table 2 that CRO_2 decomposes at 427°C, and in CRO_3 fusion occurs at 187°C and vaporization at 727°C. Fusion occurs in the more stable Cr_2O_3 and Cr at temperatures near 2, 000°C. The fourth point indicates that the thinner Cr films which have a higher precentage of Cr oxide are more susceptible to a phase change via fusion or decomposition. The extent of the diffusion of thermal energy seems to be pointed out very clearly. The fifth point again suggests the diffusion of thermal energy from the cathode with the highest temperature being at the constriction at the cathode. Since all of these measurements were taken in an oxygen containing atmosphere, it is likely that the reactions that take place also include the oxidation of Cr and subsequent phase changes.

Life tests amounting to 7, 000 device hours have been conducted using the low-current threshold elements. A dc current of 0. 5 mA was used to illustrate a safe range of operation. No failures occurred during the tests.

The etched Cr films deposited under high vacuum conditions also exhibited both the electromigration and phase change characteristics. It was found, however, that much lower resistance occurred and higher currents were required to cause current interruption. Furthermore, when any of the constricted Cr films were sintered in nitrogen or air at 350°C, initiation of

TABLE 3

REPRESENTATIVE FUSIBLE LINK MEASUREMENTS AND CALCULATIONS

Wafer No.	Sheet Resistivity	Thickness	Voltage Barrier	Fuse Resistance	Pulse Voltage	Fuse Current	Current Density	Fuse Power	Total Power	Power Density	Probable Fusing Mechanism
	ρ_s	z_M	V_B	R_F	V_g	I_f	J [1]	P_f	P_T	P_A	
	ohms/sq	A	volts	Kohms	volts	mA	$10^6 \frac{amp}{cm^2}$	watts	watts	$10^5 \frac{watts}{cm^2}$	
A. Constricted Cr Film on Al Contact Pads											
CX45 (Washout)	50	500 [3]	0	1.4	20	10.5	0.84	0.155	0.210	0.062	Electromigration and Phase Change
CZ32 (Washout)	100	400 [3]	0	2.1	28	10.8	1.08	0.25	0.30	0.10	Electromigration and Phase Change
CX47 (Washout)	400	200 [3]	0	18	42	2.2	0.44	0.09	0.092	0.036	Electromigration and Phase Change
CZ46 (Etched)	50	635	0 to 4	0.3	47	59	3.7	1.11	2.96	0.44	Electromigration and Phase Change
CZ46 (Etched and sintered) [4]	50	635	0	0.3	53	66	4.2	1.29	3.44	0.52	Fusion
B. Planar Cr Film With Al Contact Pads											
CZ37 (Etched)	100	400 [3]	0	0.46	50	50	10	1.15	2.5	2.4	Physical Stress and Rupture
CZ37 (Etched and sintered) [5]	100	400 [3]	0	0.75	28	22	4.4	0.36	0.60	0.77	Physical Stress and Rupture
CZ39 (Etched)	400	200 [3]	0	1.24	47	27	10	0.9	1.27	1.9	Physical Stress and Rupture
C. Constricted Al Film on Al Contact Pads											
CZ2 (Washout)	<1	500 [3]	0 to 7	0.020	30	57	9	0.065	1.7	0.026	Electromigration
CZ2 (Washout and sintered) [6]	<1	500 [3]	0	0.013	42	80	13	0.08	3.4	0.032	Electromigration
CY97 (Etched)	<1	250 [3]	0	0.20	6.3	8.8	2.8	0.02	0.06	0.01	Electromigration
CY97 (Etched and sintered) [5]	<1	250 [3]	0	0.13	7.8	12	3.8	0.02	0.09	0.01	Electromigration

NOTES:
1. Current density calculated for planar portion of film - a figure of merit.
2. Power density calculated from entire fusible link surface area.
3. Approximate film thickness from previous calibration of z_m versus ρ_s.
4. Sintered at 350° C for 10 minutes in N_2.
5. Sintered at 410°C in N_2 for 10 minutes.
6. Sintered at 510°C in N_2 for 10 minutes.

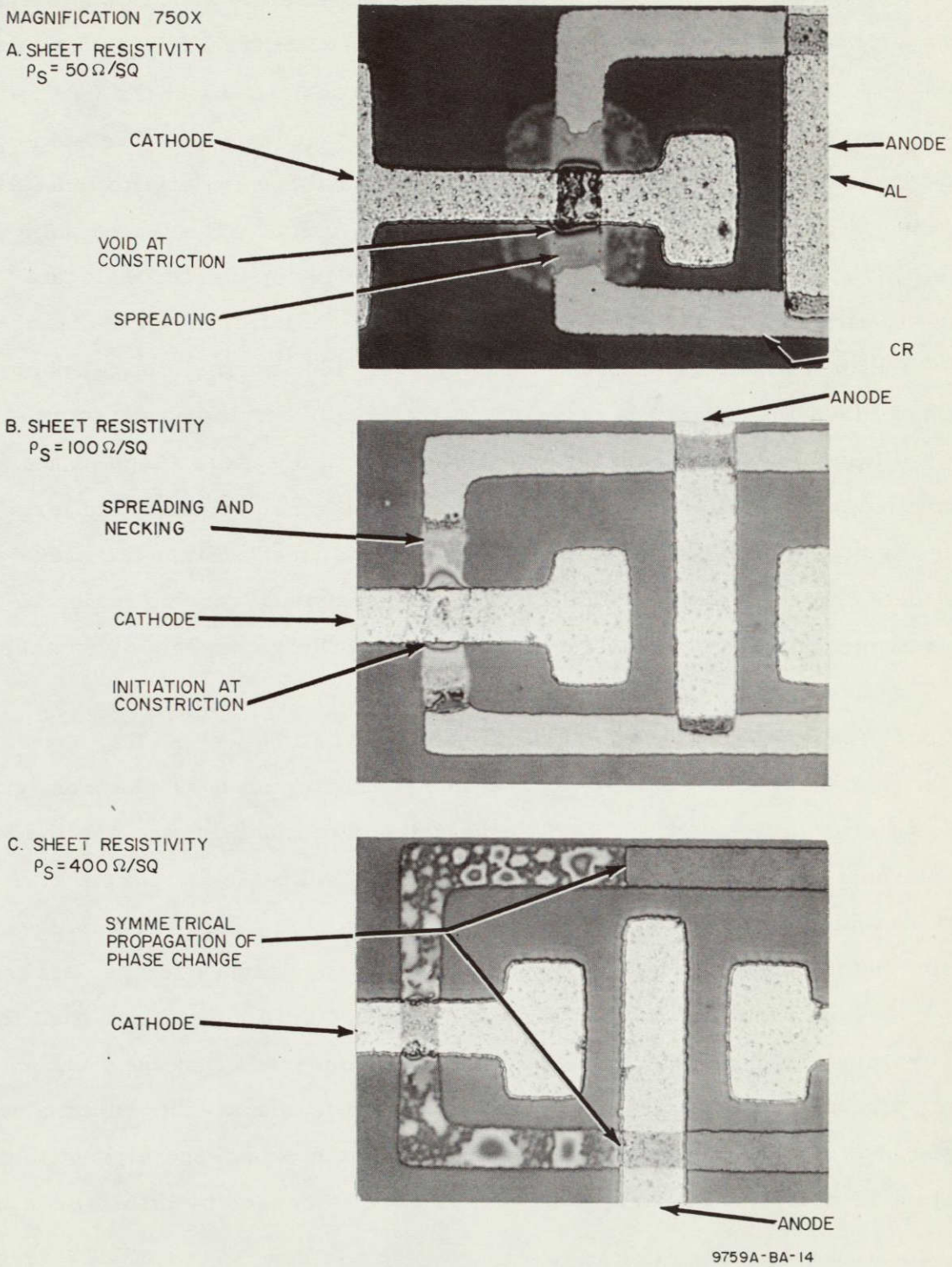

Figure 10. Photograph of Constricted Cr Film on Al Contact Pads (Washout Technique)

fusing took place randomly at both cathode and/or anode, indicating that electromigration was no longer a dominant mechanism. A scanning electron-beam microscope (SEM) was used to photograph at high magnification some of these sintered fusible links.[15] The point of constriction in the Cr film before fusing is shown at 6800 x magnification in figure 11A. The same point is shown after fusing in figure 11B. In this case there is definite indication that the Cr and the thicker Al film experienced fusion. The fusion point in Al is 658°C. The temperature of fusion may be lower than this since a solid solution of Cr and Al probably formed. A dark field optical photograph at 1500 x magnification is shown in figure 12A, and a normal optical photograph at 600 x magnification is shown in figure 12B for the same sample. The following are significant: both cathode and anode were fused at the point of constriction, propagation along the film is not evident, and large voids formed in both the Al and Cr films. It is suspected that the heat treatment causes the more stable Cr_2O_3 to be formed, forcing fusion to occur at much higher temperatures. The temperature probably was about 700°C in this case.

2.2.5.2 Planar Cr Fusible Link with Al Contact Pads

The planar Cr film does not exhibit any characteristics of electromigration as shown in figure 13. The fuse resistance is much lower, and the fusing currents are much higher as shown in part B of table 3. Note that because of smaller geometry and the high currents, very high surface power density (thermal flux) occurred, giving rise to much higher temperatures. It is estimated from the theory that with $P_A = 2.4 \times 10^5$ watts/cm^2 that the temperature could reach 1,700°C. It has been observed that the film becomes discontinuous in an abrupt lightening-like manner. The rupture occurred near the center of the film where one would expect the highest temperature to exist. It is thought that the fissure is caused by differences in

15. The SEM photographs were taken by R. Anstead of QAD at the Goddard Space Flight Center, NASA, (Greenbelt, Maryland).

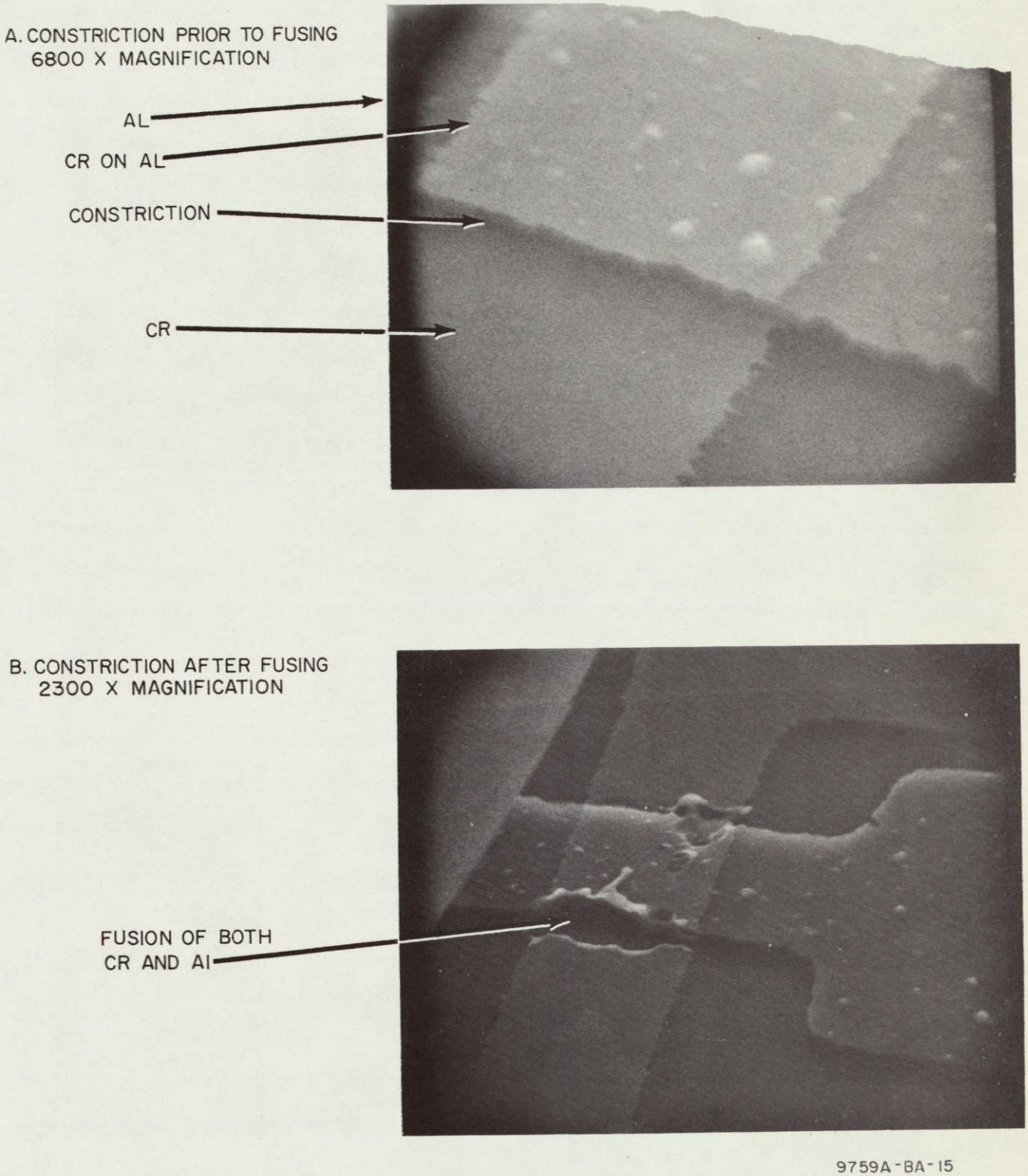

Figure 11. Photograph Using SEM of Constricted Film on Al Pad Before and After Fusing (Etched and Sintered)

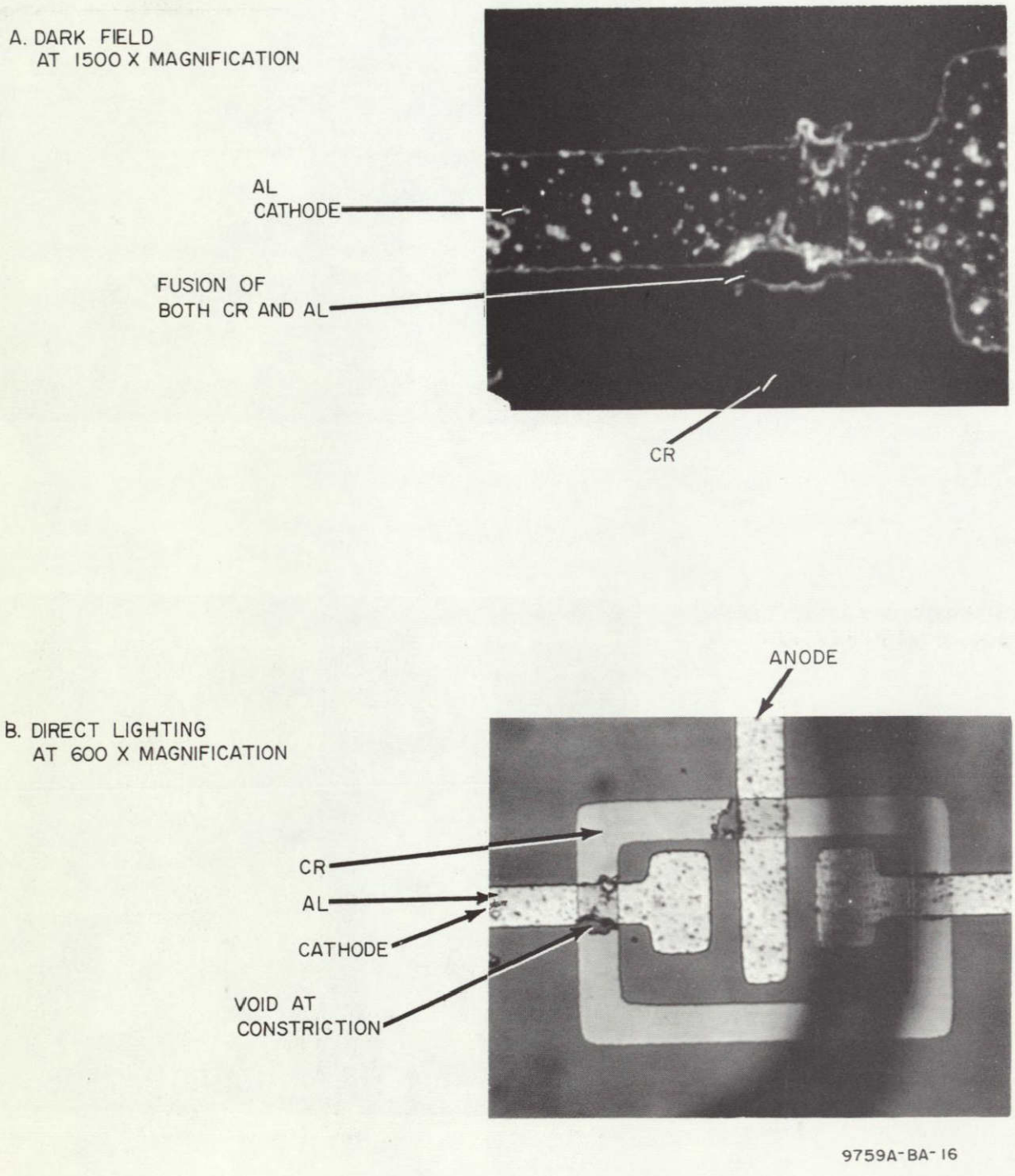

Figure 12. Photomicrograph of the Same Location Shown in Figure 11

the coefficients of expansion between the metal film and the silicon dioxide at a high temperature. Sintering at 450°C for 10 minutes in nitrogen reduces the current required and the power density significantly.

2.2.5.3 Constricted Al Films on Al Contacts

Thin Al films were deposited on thicker Al contact pads to obtain constricted Al fusible links similar to the etched Cr constricted films. The measurements and calculations for representative samples are shown in table 3, part C. Note that very high current density was required to achieve current interruption. Micrographs of voids, that occurred consistently at the cathode when pulsed, are shown in figure 14. This evidence points to electromigration of Al rather than fusion; however, the power density at the constriction is probably high enough to cause fusion if the migration is not complete. These constricted Al films often were open circuits prior to testing and therefore seem more difficult to build in a reproducible manner.

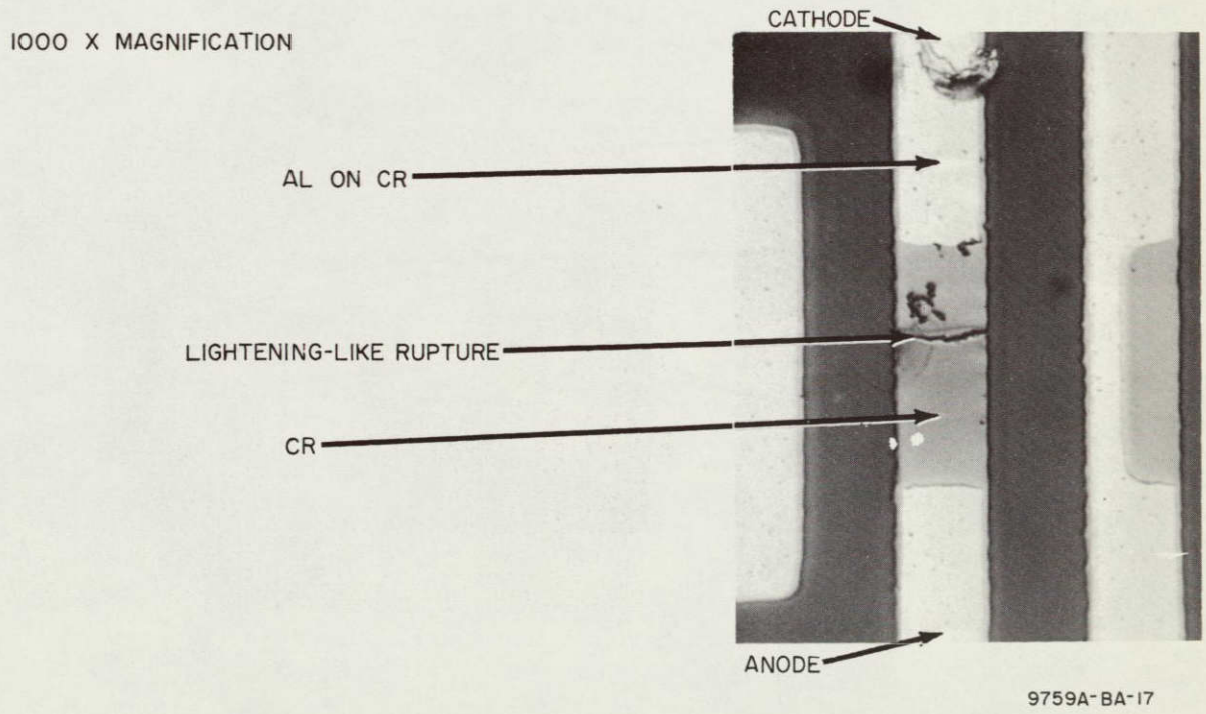

Figure 13. Photomicrograph of Planar Cr Film on Al Contact Pass

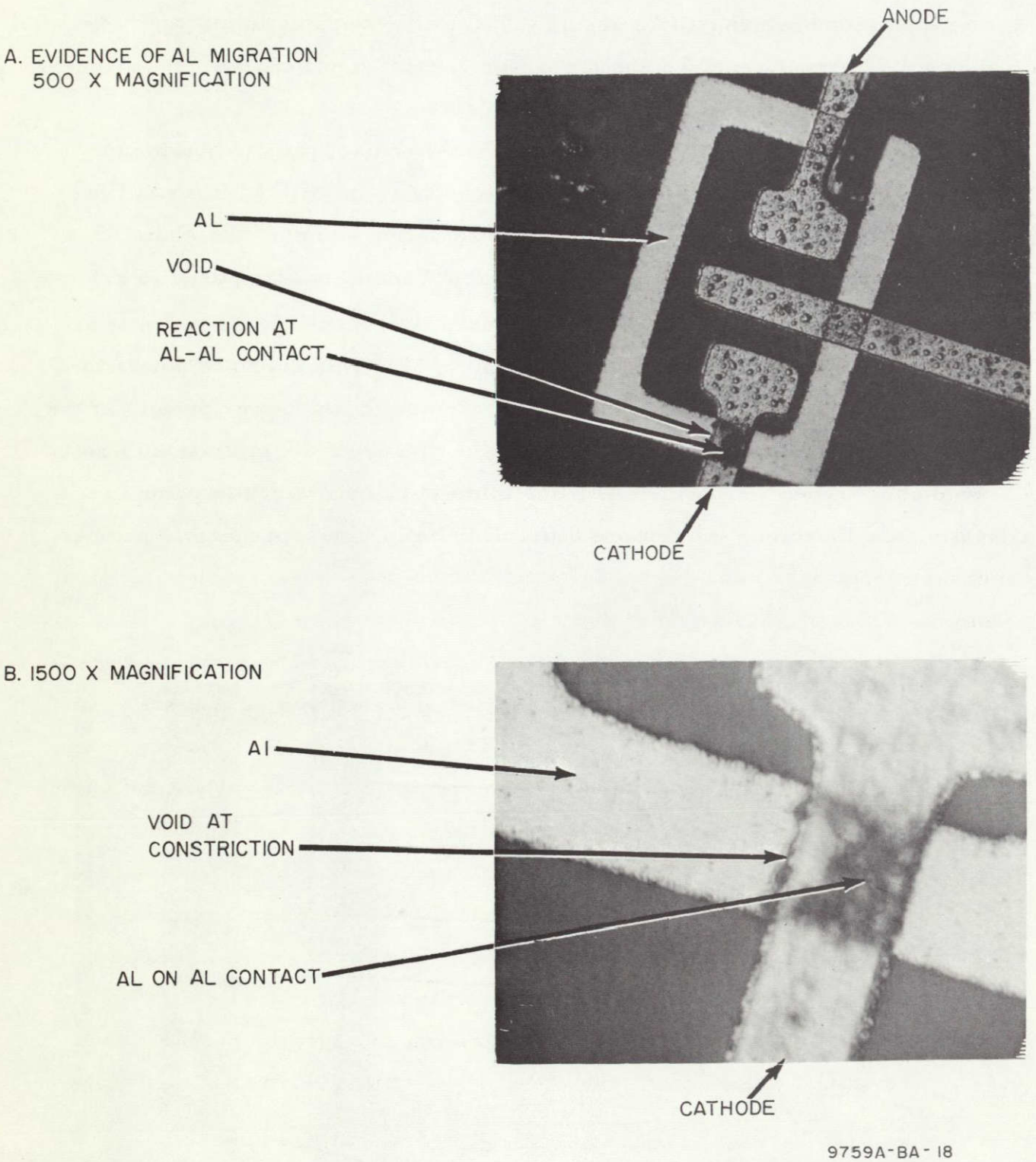

Figure 14. Photomicrograph of Constricted Al Film on Al Contact Pads

2.2.5.4 Electromigration Experiments

The data summarized below was obtained in the following manner. Silicon substrates having aluminum interconnects 0.5 mil wide and 1000 Å thick were heated by means of a strip heater. A dc current was then passed through the interconnects and observed on a Tektronix curve tracer. The temperature as reported is read from a thermocouple placed in an aluminum block below the wafer. This technique does not allow for heat losses or I^2R heating. The highest power dissipated is 0.25 watt and occurs in the room temperature measurements. Estimation of the thermal impedance to be 150°C per watt yields a temperature rise of 37.5°C. This is a rise of 12.5 percent of the absolute temperature. For the higher temperature measurements this error is smaller. The current interrupt time τ_I is observed as a function of temperature and current level with the current density being computed using the measured dimensions. The thickness measurements were made by measuring electronically the step distance from the substrate to the top of the thin film using a Talysurf.

In the course of these measurements, observations of the current interrupt time as a function of current density were made as the temperature was cycled between room temperature and 215°C and duplicated. The indications are that the data is repeatable even with the thermal cycling. The conclusion then is that current and high temperatures together are required to observe the effects. The results of these measurements are summarized for aluminum in figure 15. Subsequent measurements were made for chromium interconnects and are summarized in figure 16. As in the case of aluminum the results are indicative of the same type of behavior.

In summary from the dc experiments, the interrupt time τ_I as a function of current density with temperature as a parameter for aluminum has been found to be

$$\ell n\ (\tau_I) = -\alpha\ (T)\ \ell nJ + \beta\ (T) \tag{36}$$

where

$$\alpha\ (T) = \frac{6,490}{T} - 9.730 \tag{37}$$

and

$$\beta\ (T) = \frac{1.09 \times 10^5}{T} - 162.0 \qquad (38)$$

The relationship

$$\ell n\ (\tau_I) = -\alpha\ (T)\ \ell nJ + \beta\ (T)$$

also exists for chromium, but the slope is less sensitive to temperature. Due to the limited amount of data collected for chromium, calculations of α (T) and β (T) are not available.

Finally, the typical current density under pulse conditions has also been shown in figure 15 and 16 for planar and constricted films. Note that the pulse data for the planar Cr films for the same sample agrees with the extrapolation of the dc data, while the data for the constricted films is an order of magnitude lower.

2.3 OXIDE BREAKTHROUGH MEMORY ELEMENTS

In addition to the fusible link memory elements, oxide breakthrough elements were considered for use as read-only memory elements. The oxide breakthrough element is initially in a high-impedance state corresponding to a logic level. Upon the application of a voltage which produces an electric field in the oxide greater than the critical breakdown field, the metal oxide semiconductor element is brought to basically an irreversible low-impedance state corresponding to a second logic level. The theory of the breakdown and subsequent low-resistance state is discussed along with the experimental observations and results in the following sections.

2.3.1 Oxide Breakdown Mechanisms

Oxide breakdown in metal-oxide-semiconductor structures is related to the thermal conditions under high electric field conditions. Furthermore, it has been shown that electrical conductivity in insulators is made up of several components as listed below:

a. Field-enhanced thermal excitation of trapped electrons (Poole-Frenkel effect)

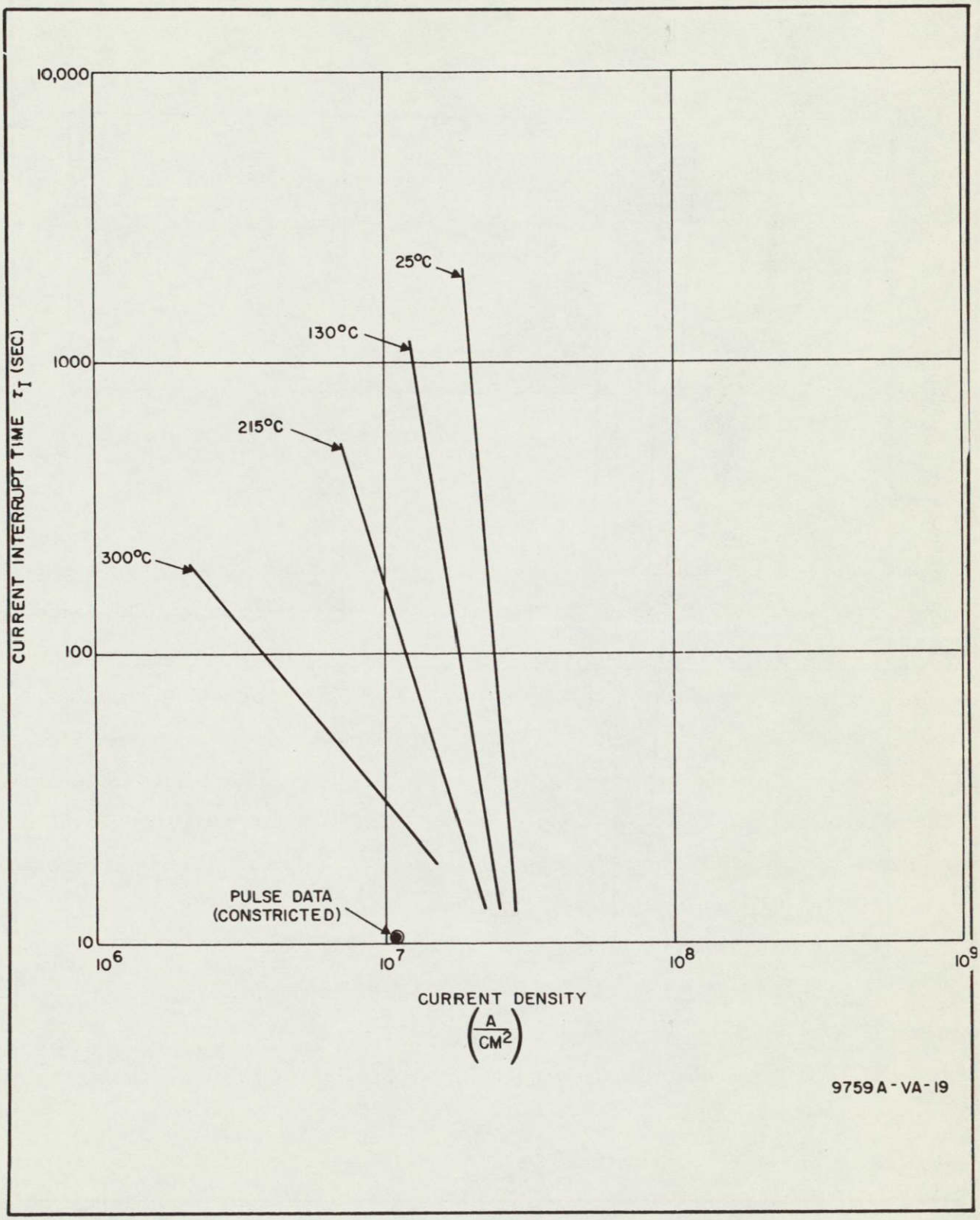

Figure 15. Planar Aluminum Film (1000 Å Thick)

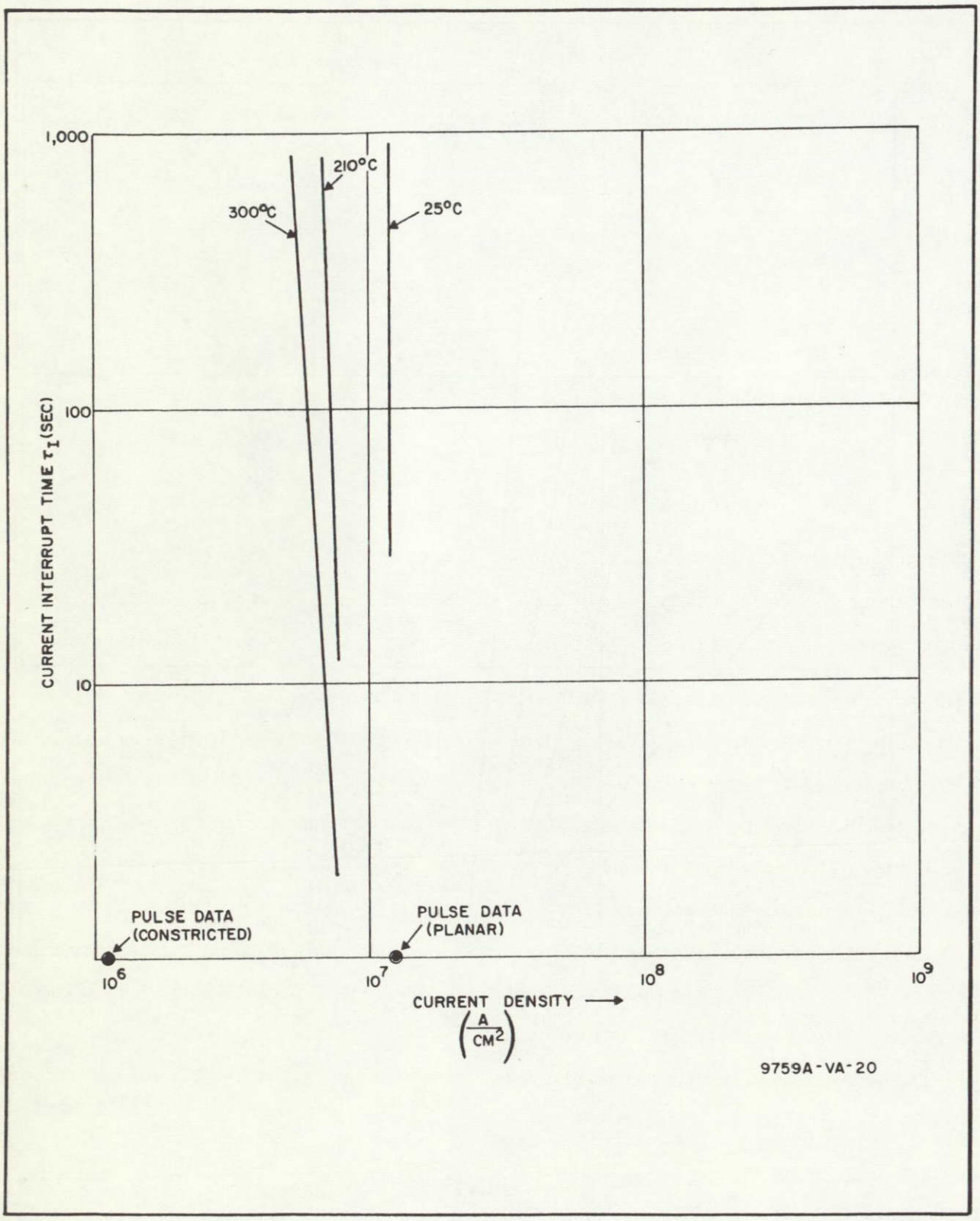

Figure 16. Planar Chromium Film (200 Å Thick)

$$J_1 = C_1 \, E \exp \left\{ -q \left[\Phi_1 - (qE/\pi \, \epsilon_o \, \epsilon_d)^{1/2} \right] / kT \right\}$$

b. Tunneling (Fowler-Nordheim emission)

$$J_2 = C_2 \, E^2 \exp (-E_2/E)$$

c. Hopping or thermally excited electrons (ohmic)

$$J_3 = C_3 \, E \exp (-q \, \Phi_3/kT)$$

d. Thermally excited ions (ionic conduction)

$$J_4 = C_4 \, \frac{E}{T} \exp (-q \, \Phi_4/kT)$$

Measurements of current in silicon dioxide under high field conditions indicate that the field-enhanced thermal emission (Poole-Frenkel) component dominates.[16] Current densities as high as $1 \frac{A}{CM^2}$ have been measured for SiO_2 at electric fields of 10^7 V/cm under pulse conditions. The power density under these conditions is 10^7 watts/cm^3. The temperature increase of the film is estimated from the thermal model developed for the fusible links as negligible for the 0.1 micrometer film. At this low temperature, only localized changes in the film such as generation of an ionized plasma, or thermally enhanced current runaway at nonhomogeniety can explain the breakdown current. Any localized increase in current density will result in a runaway condition both thermally and electrically. Usually, the breakdown occurs at the weakest point in the oxide.

These runaway conditions after oxide breakdown, for the case of unlimited

16. S. M. Sze, "Current Transport and Maximum Dielectric Strength of Insulating Films," J. App Phys, XXXVIII, No. 7, (June 1967), 2951.

input currents, have been reported.[17] For unlimited current supply the very high power dissipation results in temperature in excess of 4,000° K and volatilization of the materials involved. This type of unlimited breakdown can propogate and destroy the junctions in integrated circuits.

The major difference between this type of breakdown event and the events studied for the oxide memory element is that the current after breakdown is controlled both in magnitude and time. Thus, the limited energy input prevents catastrophic destruction of surrounding oxide and junctions.

2.3.2 Experimental Approach

The oxide breakthrough memory element experiments were designed to be compatible with MOS integrated circuit fabrication. A cross section of a typical oxide breakthrough element is shown in figure 17.

The variables in the experiments were crystal orientation, diffused junction, dopant type (N^+ or P^+), oxide thickness and metal type.

The pulse test conditions are also shown in figure 17. The generator resistance was varied between 0.5 and 10K Ω to limit the current at different levels. The pulsewidth was 10 to 100 microseconds.

2.3.3 Observations and Results

The most significant observation in the tests was that with the current input controlled in time and magnitude such that the energy input was limited, the breakdown events were singular for each given capacitor. Also, the breakdown point was of minimum size, typically 0.5 micrometer, and did not destroy the surrounding oxide and junction regions. A photograph of a typical 300-Å oxide breakthrough point is shown in figure 18.

Only a singular point of breakdown occurred in the 300-Å oxide with the application of 35 V through a 0.5KΩ resistor. The cracked glass extensions occurred if an overvoltage of 50 watts was applied.

---

17. N. Klein, "The Mechanism of Self-Heating Electrical Breakdown in MOS Structures, " "IEEE Trans in Elect., ED-13, No. 11 (November 1966), 788-805.

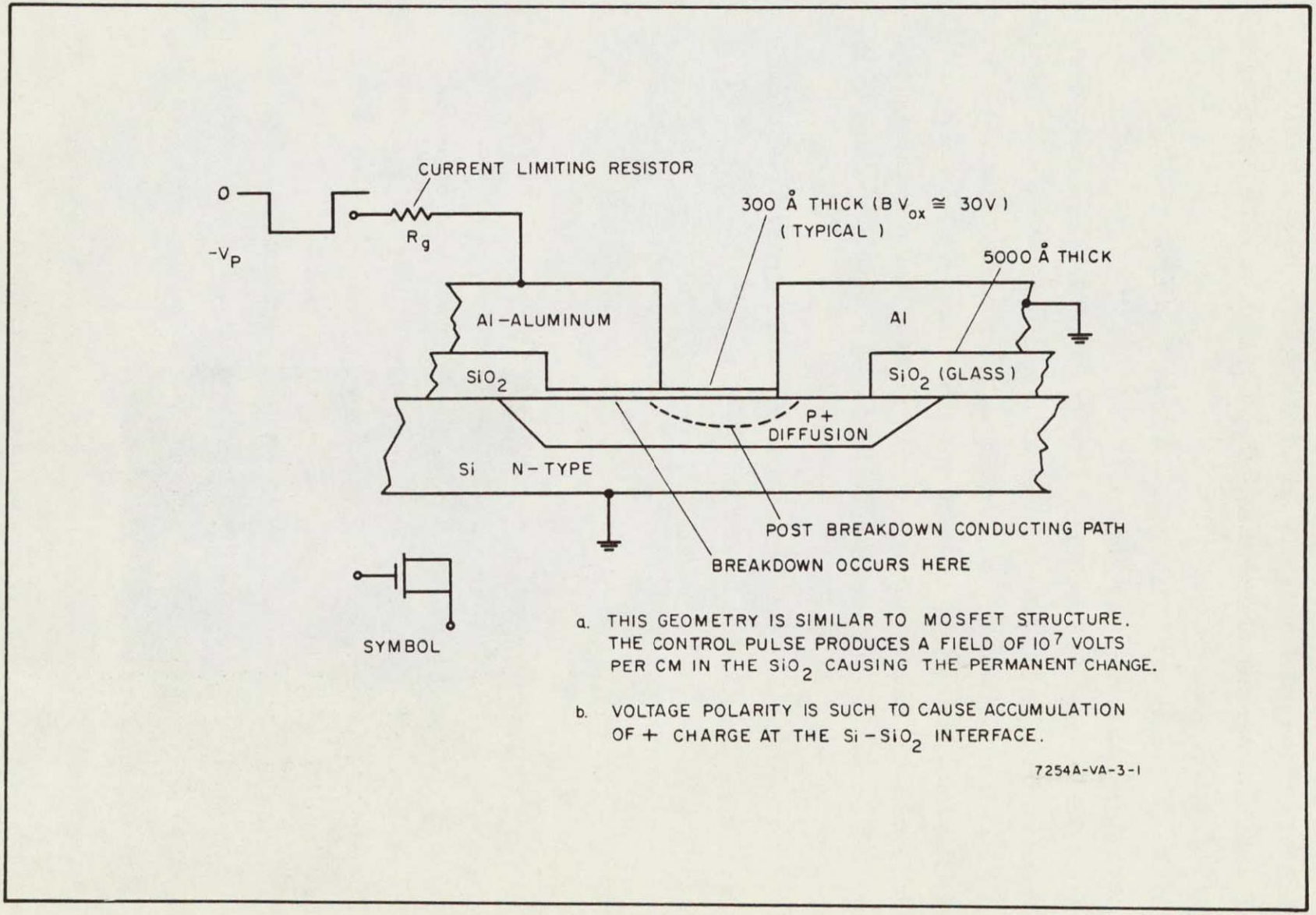

Figure 17. Cross Section of Permanent Oxide Breakdown Connection

The results of the pulse tests and subsequent contact measurements for typical oxide breakthrough elements are shown in table 4. The following is a list of significant observations.

a. Breakthrough of an aluminum - SiO_2 - P^+ silicon structure forms a uniform, linear, ohmic contact.

b. Breakthrough of an aluminum - SiO_2 - N^+ silicon structure forms a nonlinear ohmic contact. (Since Aℓ is a p type dopant, it forms a junction.)

c. Uniform and reproducible breakthrough voltages of 30V and 20V for 300- and 200-Å oxides respectively where obtained on P^+ silicon.

d. Positive voltage on metal electrode of MOS structure has approximately 5 volts lower breakthrough voltage than for a negative voltage on the metal.

e. The resistance of the formed pipe generated during oxide breakthrough has been calculated to be 100Ω to 170Ω.

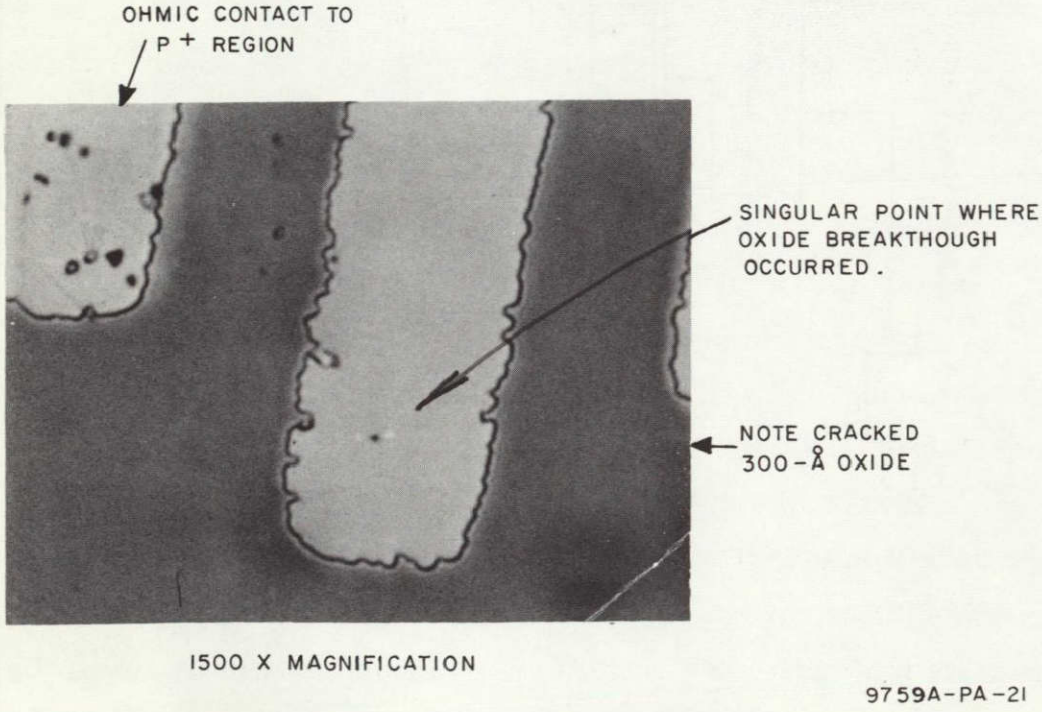

Figure 18. Photomicrograph of Oxide Breakthrough Point

TABLE 4

PULSE TEST RESULTS AND CONTACT MEASUREMENTS

WAFER NO.	Z_{ox} Å	VOLTAGE APPLIED TO METAL + VOLTS	VOLTAGE APPLIED TO METAL - VOLTS	DIFFUSION TYPE	CONTACT CHARACTERISTICS AFTER BREAKTHROUGH LINEARITY	CONTACT CHARACTERISTICS AFTER BREAKTHROUGH RESISTANCE OHMS
CZ79	300	34		P^+	YES	140
CZ79	300		38	P^+	YES	200
CZ83	200	30		N^+	NO	250 - 1,000
CZ76	200	20		P^+	YES	130

9759A-TA-22

f. The diameter of the electrically formed pipe has been measured to be approximately 5000 Å in diameter.

g. The current density during pipe formation has a maximum value of 2×10^7 A/cm^2.

h. A series resistance above 1KΩ can inhibit pipe formation during the electrical breakthrough operation.

i. Life tests with 0.5 mA through the Al-SiO_2 - P^+ Si breakthrough element show stability, linearity, and uniformity throughout the test. A 14,000 device-hour test was completed during this program with no failures.

2.4 POLARIZABLE MNOS MEMORY ELEMENTS

Multiple insulator structures such as the silicon nitride-silicon dioxide type have been found to exhibit polarization with the application of large electric fields. The charge introduced by the large electric fields becomes trapped within the nitride and thus does not exhibit dielectric relaxation typical of ferroelectrics. However, thermal excitation and normal applied working voltages gradually remove the charge over a long period of time.

A typical MNOS field effect transistor exhibits a change in threshold voltage with applied polarizing voltage as shown in figure 19.

Since the MNOS element is not truly nonvolatile for periods greater than several thousand hours, greater emphasis was placed on the nonvolatile fusible link and oxide breakthrough for applications where hard fixed program storage is required.

2.5 READ-ONLY MEMORY ORGANIZATION

2.5.1 Overall System Organization

Ultimately the read-only memory organization is to be designed to be compatible with the complementary MOSFET memory described in paragraph 2.1. Four address inputs, a basic read command, 100 date line outputs, and B^+ and ground are required for a total of 23 leads minimum. The variations in read-only memory cell arrangements described in the next paragraph were assembled and tested using the fusible link and oxide breakthrough memory elements fabricated in the course of the read-only memory program.

2.5.2 Basic Permanent Memory Cells

Different circuit requirements are imposed by the different memory elements, as well as the basic requirements of the overall system and the limitations imposed by the complementary MOSFET fabrication techniques. In each of these techniques to follow, all factors were taken into consideration including the MOSFET characteristics and associated junction isolation available.

2.5.2.1 Memory Cell Using Fusible Interconnections

The least complicated memory cell schematic that meets all of the requirements and uses one or the other of the fusible interconnection techniques is shown in figure 20. The sequence of operation for this memory cell is the following:

a. ROM energized with maximum possible supply voltage (+20 volts desirable)

b. Data set on each data line

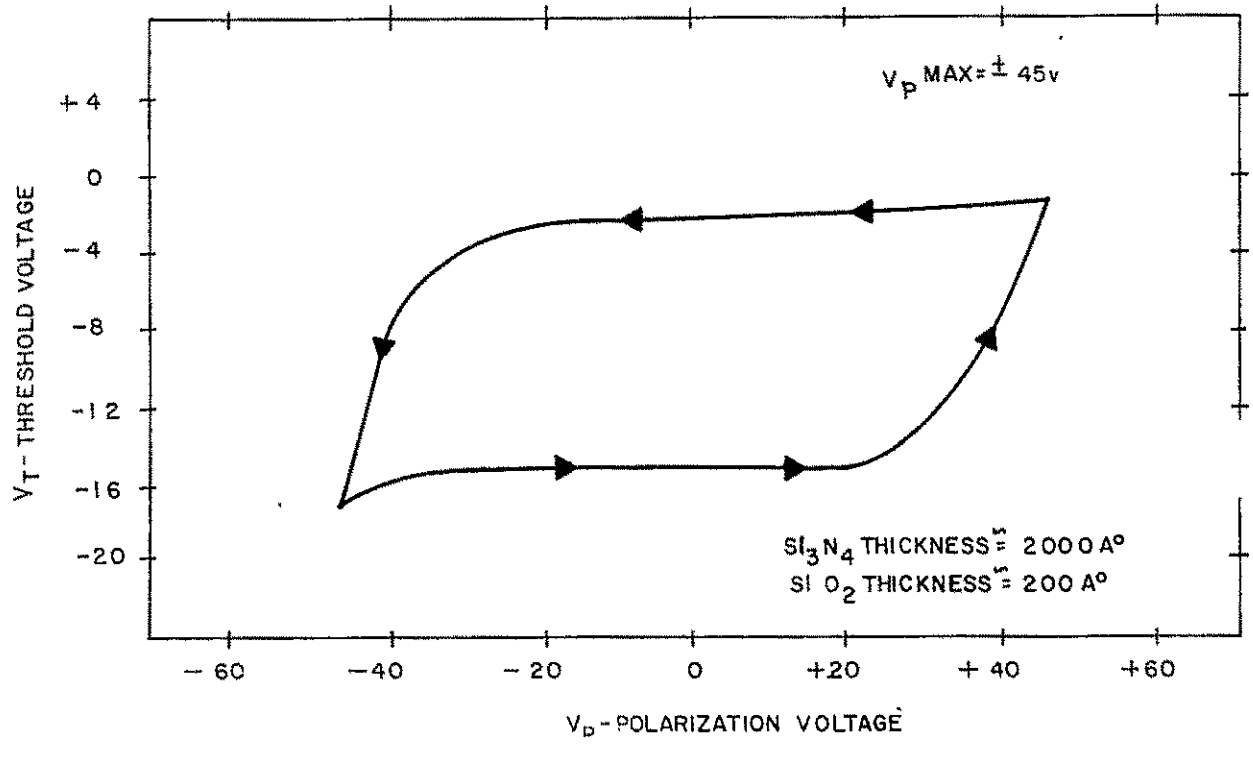

NOTE: THE SAME ELECTRIC FIELD THAT PRODUCED THE ABOVE CHANGES CAN BE ACHIEVED WITH THINNER LAYERS AND LOWER POLARIZING VOLTAGES.

7254A-VA-4

Figure 19. Polarizable Si_3N_4 - SiO_2 FET Characteristics

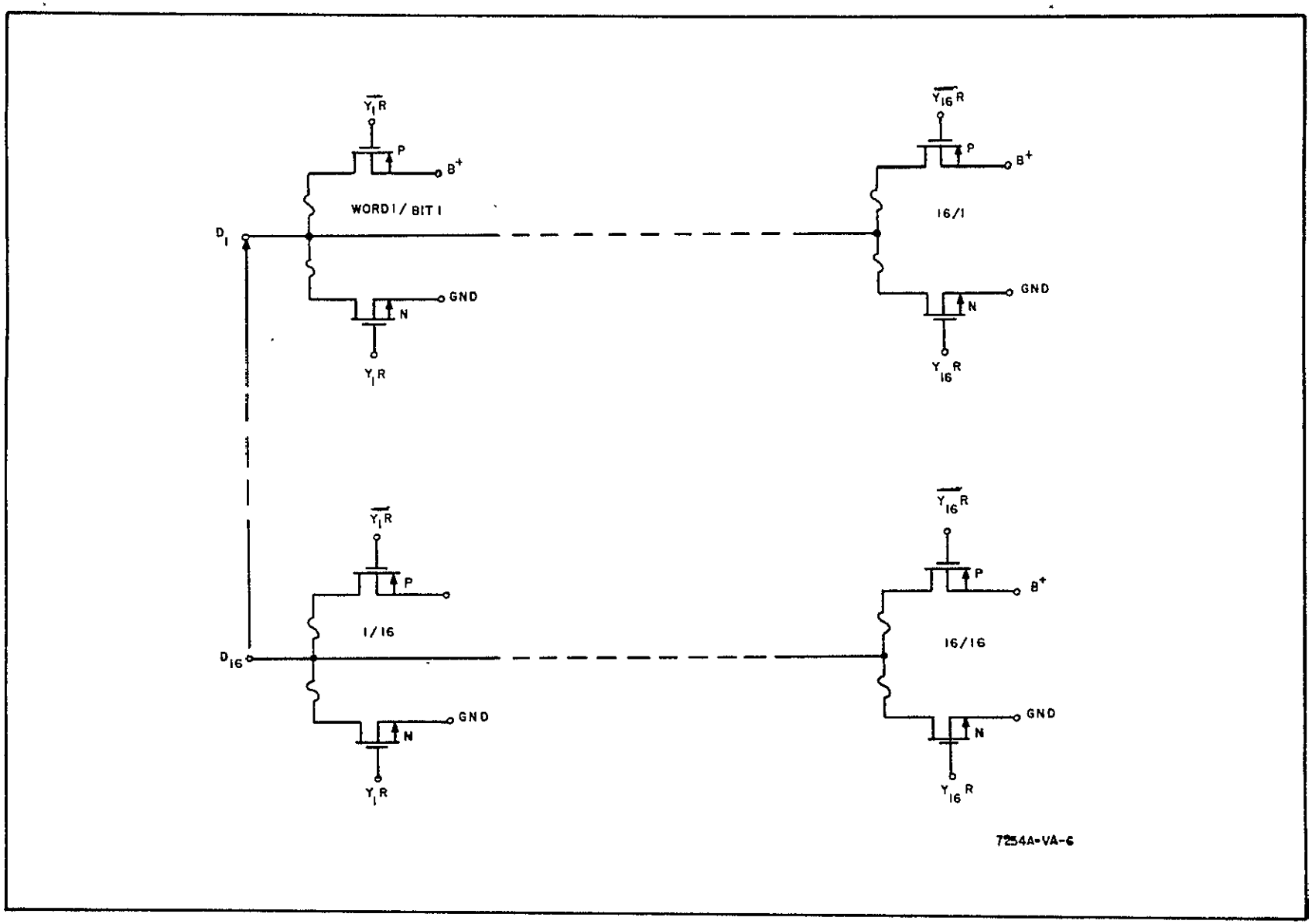

Figure 20. Fusible ROM Schematic

c. Address selected and read command presented

d. Current flows from memory B^+ to ground on data lines, through the fuse and the p channel MOSFET, where 0 set in; the current flows from B^+ on the data line to memory ground through the fuse and the n channel MOSFET where 1 set in

e. Remove read and repeat cycle for next address.

No current flows through the devices that have not been addressed. The data line source resistance must be much lower than internal branch resistances to prevent current flow through the parallel branch during the write cycle. It can be seen that the fuses have been opened in the B^+ branch where 0 has been written in and opened in the ground branch where 1 has been written in. Therefore a 0 is read out where 0 was written in and 2 read out where 1 was written. Automatic equipment could be used to program the memory. Current sensing could be used to indicate when the fuse was blown.

2.5.2.2 Memory Cell Using Oxide Breakdown

The memory cell using oxide breakdown techniques is shown in figure 21. This memory cell requires a more complicated sequence and a few more leads than the fusing technique; however, the steps can still be easily automated. More MOSFETS are required; but they can be of smaller size; and, therefore, a memory cell area of 50 square mils can be easily met. The sequence of operation for this memory for a typical oxide breakdown voltage of 30 volts is the following:

Write Sequence

a. Apply $B^+ \cong 15$ V

b. Set V_3 at $(BV_{ox} - B^+ + 2\,|V_{TP}|) \cong -21.0$ volts and V_1, V_2 at 0 volts

c. Address all words and set all data lines to 0 volts to remove any accumulated charge on capacitors

d. Remove address on all words; open all data lines

e. Address word to be written into

f. Set data lines

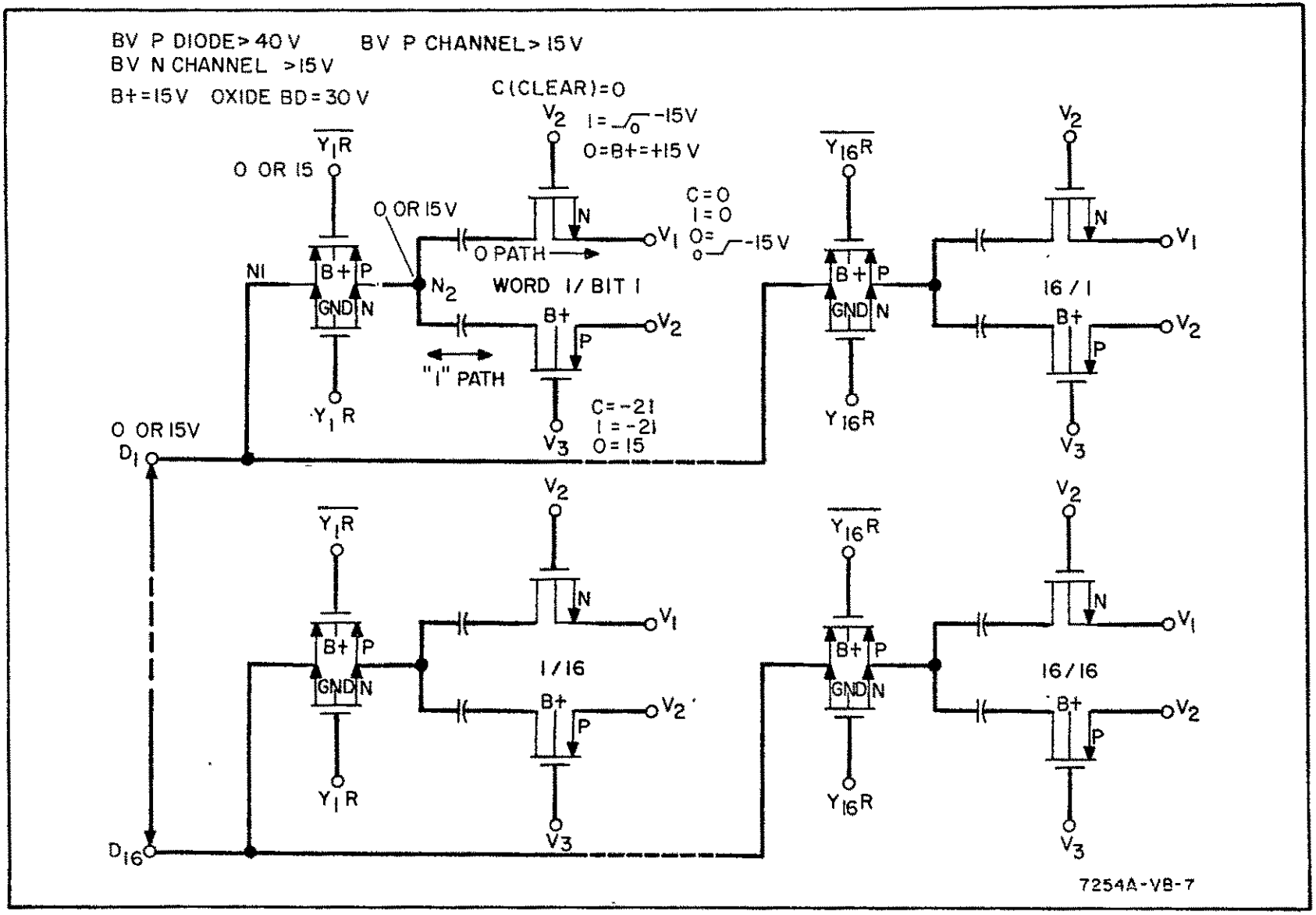

Figure 21. Oxide Breakdown ROM Cell Schematic

g. Change V_2 to $-(BV_{ox} - B^+) > -15$ volts gradually until logical 1 (B^+) capacitors breakdown; monitored current automatically resets V_2 to 0 volts

h. Complement data inputs

i. Change V_1 to $-(BV_{ox} - B^+) > -15$ volts gradually until logical 0 (0 volts) capacitors breakdown; monitored current automatically resets V_1 to 0 volts ($V_2 = 0$, $V_3 = 21$).

Repeat steps e through i for next word.

Read Sequence

a. Set V_2 at B^+; V_1 and V_3 at 0 volts

b. Apply B^+

c. Address word and read.

Less complicated circuit schemes based on one transistor per cell can be achieved if precharging of the data line driver is utilized. Therefore, only one transistor per cell is required for the fusible link and two per cell for the oxide breakthrough cell. Also the MOS transistor elements can be replaced with diodes if the programming voltages and currents are contained in the address commands. The memory cells diagrammed in figures 20 and 21 which give dc + 10 and 0 V logic levels from low-impedance MOS transistors were tested and shown to be operable as described.

3. CONCLUSIONS AND RECOMMENDATIONS

Electrically programmable MOS transistor read-only memory cells have been constructed using low-current threshold chromium - chromium oxide film memory elements and low-voltage breakdown aluminum-silicon dioxide - p + diffused silicon memory elements. Fabrication and operation of these memory elements, using technology consistent with MOS array technology, is possible.

Low-current threshold fusible link elements having pulse current thresholds of less than 10 mA and current interrupt times of less than 100 microseconds were achieved, although the physical configuration was not optimized. The most reproducible low-current threshold was obtained using the constricted Cr - Cr oxide film an Al contact. The conclusion is that the low-current threshold is principally the result of the high-temperature, accelerated electromigration at the constriction. The heat-transfer analysis, the tendency towards localized thermal runaway, and the repeated evidence of migration from the cathode support this conclusion. Both the planar Cr and planar Al elements may also be made to have low-current thresholds by increasing the power dissipation per unit area and the thermal resistance through geometry and film resistance control. However, the fusing mechanism tends towards the higher temperature process of metal fusion which has a higher probability of adversely affecting the underlying oxide.

The recommendation is made that the fusible link development be continued to optimize and extend the design and technology base for large scale integrated arrays.

Oxide breakthrough memory elements having reproducible breakdown voltages of 20 volts for 200-A° oxides were achieved. By controlling the

energy of the breakdown pulse, single-breakthrough points of 0.5 micrometer diameter occurred. This technique resulted in the preservation of the surrounding oxide and junction regions. The ohmic contact formed to the p + diffused region after breakdown was shown to be reliable by life tests. The conclusion is that the oxide breakthrough element can be used as a memory element; however, adequate protection against voltage transients must be included in the integrated circuit. The memory cell circuitry for the oxide breakthrough element is somewhat more complex than for the fusible link element. The oxide element is therefore, less attractive for memory arrays with parallel write. However, if each bit is programmed individually; either by the programmer or in a single-bit, 256- address, memory configuration; the circuitry is no more complicated than for the fusible link.

4. NEW TECHNOLOGY

In accordance with the new technology clause of the subject contract, we report that, to the best of our information and belief, the items conceived or first reduced to practice in the performance of this contract are the following:

Disclosure No. AA68-318 (Westinghouse Case No. 40,578) by J. R. Cricchi, W. J. Lytle, D.S. Herman entitled "Integrated Fusible Intraconnections"

Disclosure No. AA69-101 by J.R. Cricchi, W.J. Lytle entitled "Nonvolatile Read/Write Memory Element"

Disclosure No. AA69-103 by J.R. Cricchi entitled "Diode Matrix Memory Array."

It is further reported that to the best of our knowledge there were no subcontracts containing the new technology clause awarded during the course of the contract.

Abstracts of the above disclosures are included on the following pages.

4.1 INTEGRATED FUSIBLE INTRACONNECTIONS

Disclosure No, AA68-318 (Westinghouse Case No. 40,578) by J.R. Cricchi, W. J. Lytle and D.S.Herman.

Integrated fusible intraconnections made of a single metal or different metals which depend on defect accelerated electromigration phenomena have advantages over fusible links which require joule heating for melting or volatilization. These elements may be used in programmable nonvolatile LSI memory arrays.

4.2 NONVOLATILE READ/WRITE MEMORY ELEMENT

Disclosure No. AA69-101 by J.R. Cricchi and W.J. Lytle.

A nonvolatile read/write memory having a limited number of programming cycles can be achieved through the use of vertical fusible links in series with

oxide breakthrough elements. A 1024 Bit Memory with the capacity of 625 Programming Cycles in a 100 by 100 mil chip seems possible. The high density (10 millibar per square inch) memory appears to offer a virtually indestructible, radiation-resistant memory for main stored programs in digital systems.

4.3 DIODE MATRIX MEMORY ARRAY

Disclosure No. AA69-103 by J.R. Cricchi

Bidirectional buffers on the memory data line with diode matrix addressing of fusible link or oxide breakthrough memory elements provides higher density transient protected memory arrays.

BIBLIOGRAPHY

Black, J. R., "Metalization Failure in Integrated Circuits," "Technical Report No. RADC-TTR-67-477," September 1967.

Blech, I. A. and H. Sello, "The Failure of Thin Aluminum Current-Carrying Strips on Oxidized Silicon," Physics of Failure in Electronics, 5, 1967, pp. 496-505.

Bosvieux, C. and J. Friedel, "Sur L' Electrolyse Des Alliages Metalliques," Journal Phys Chem Solids, 23, 1962, p. 123.

Condon, E. H. Odishaw, ed., Handbook of Physics, New York; McGraw-Hill, 1967, pp. 4-74-4-78.

Carslaw, H. S. and J. C. Jaeger, Conduction of Heat in Solids, Oxford: Oxford Press, 1959, p. 75.

Fiks, V. B., "On the Mechanism of the Mobility of Ions in Metals," Sov Phys Solid State, 1, 1964, pp. 14-28.

Grove, A. R., "Current-Induced Marker Motion in Copper," Journal Phys Chem Solids, 20, 1961, pp. 88-93.

Ho, P. S., "Electromigration and Soret Effect in Cobalt," Journal Phys Chem Solids, 27, 1966, pp. 1331-1338.

Ho, P. S. and H. B. Huntington, "Electromigration and Void Observation in Silver," Journal Phys Chem Solids, 27, 1966, pp. 1319-1322.

Huntington, H. B. and A. R. Grove, "Current-Induced Marker Motion in Gold Wires," Journal Phys Chem Solids, 20, 1961, pp. 76-87.

Klein, N., "The Mechanism of Self-Heating Electrical Breakdown in MOS Structures," "IEEE Trans in Electrical Deviation," Ed 13, No. 11, November 1966, pp. 788-805.

O'Sullivan, D. D., "Electromigration in Aluminum and Chromium Films," "Defense and Space Center Technical Memo, D. S. C. 7796," May 14, 1969.

Penny, R. V., "Current-Induced Mass Transport in Aluminum," Journal Phys Chem Solids, 25, 1964.

Sze, S. M., "Current Transport and Maximum Dielectric Strength of Insulating Films," Journal App Phys, XXXVIII, No. 7 June 1967, p. 2951.

West, Robert C., ed., Handbook of Chemistry and Physics: Thermodynamic Properties of Elements and Oxides, Ed 49, Chemical Rubber Co., Cleveland, Ohio, 1968, D-32-D-37.